Design of an IGBT-Based Pulsed Power Supply for Non-continuous-mode Electrospinning

by

Rina Baba

A thesis
presented to the University of Waterloo
in fulfillment of the
thesis requirement for the degree of
Master of Applied Science
in
Electrical and Computer Engineering

Waterloo, Ontario, Canada, 2010

AUTHOR'S DECLARATION

I hereby declare that I am the sole author of this thesis. This is a true copy of the thesis, including any required final revisions, as accepted by my examiners.

I understand that my thesis may be made electronically available to the public.

Abstract

Nanofibres are useful in a broad range of applications in areas such as medical science, food science, materials engineering, environmental engineering, and energy and electronics due to their outstanding characteristics: their small size, high surface-to-volume ratio, high porosity, and superior mechanical performance. Recently, controlled drug delivery systems have gained significant attention, especially with respect to the use of polymer nanofibres. For these systems, the ability to control of the length of the polymer nanofibre is important because the amount of drug released depends on the length of the fibre. Electrospinning is the simplest and most cost-effective method of fabricating polymer nanofibres. In the process, a high voltage is used to create an electrified jet which will eventually become a nanofibre. The electrified jet ejects when a high voltage is applied to the electrospinning setup. On the other hand, the jet does not eject when the applied voltage is below the threshold voltage. It is therefore possible to fabricate and chop nanofibres by controlling the values of the voltages applied and a special high-voltage pulsed power supply has been developed for this purpose.

In this research, an IGBT-based pulsed power supply has been designed and built to be used for non-continuous-mode electrospinning. The IGBTs are connected in series to deliver high voltage pulse voltages to an electrospinning setup. The IGBT-based pulsed power supply is capable of producing controllable square pulses with a width of a few hundred microseconds to DC and amplitudes up to 10 kV.

The technique of non-continuous-mode electrospinning was tested using the pulsed power supply designed in this work. The new system was able to fabricate and chop nanofibres with PEO and alginate/PEO solutions. It was concluded that the minimum pulse width that can initiate an electrified jet is approximately 80 ms for the parameters used in this study. A longer period produces a more constant jet during the pulse-on voltage when the duty ratio is the same value. It is also highly likely that a jet is always ejected during the pulse-on voltage when the duty ratio is more than 40 %.

Acknowledgements

First and foremost, I would like to thank my supervisor Dr. Shesha Jayaram for her guidance and suggestion throughout my graduate studies. I am also grateful to Dr. Mehrdad Kazerani and Dr. Dayan Ban for reviewing this thesis. I also like to thank to my colleagues in the High Voltage Group for their helps, advices, and useful discussions.

My appreciation to my partner Jean and my friend Ansis who have made my student life cheerful and enjoyable.

I must thank my parents always believing in and trusting me. Also, I would like to thank my sister and brother who inspire and challenge me.

The financial support provided by Heiwa Nakajima Foundation is gratefully appreciated.

Table of Contents

List of Figures

List of Tables

Chapter 1
Introduction

Electrospinning, one of the techniques for fabricating polymer nanofibres, has been researched worldwide. However, a technique has not been established for both fabricating and chopping polymer nanofibres at the same time. A nanofibre of a well-defined length will be required for drug delivery in the next decades. This research therefore presents a technique called non-continuous-mode electrospinning with a high-voltage pulsed power supply. This chapter provides the background information necessary for an understanding of the requirements for chopped nanofibres, electrospinning, non-continuous-mode electrospinning, and high-voltage power supplies.

1.1 Requirements for producing chopped nanofibres

The term nanofibre is a combination of “nano” and “fibre.” “Nano” refers to physical quantities at the scale of a billionth of the reference unit. “Fibre” is defined from a geometrical standpoint: a slender, elongated, threadlike object or structure [1]. Therefore, a nanofibre can be considered to be a fibre with a diameter in the nanometre range.

The outstanding characteristics of nanofibres are their small size, high surface-to-volume ratio, high porosity, and superior mechanical performance. Due to these advantages, nanofibres are useful in a broad range of applications in areas such as medical science, food science, materials engineering, environmental engineering, energy and electronics [1-4].

Nanoparticles have already found important uses in drug release applications and diagnostics because the nanoscale is reflected in the biological scale, for example, in sizes ranging from that of enzymes and viruses up to bacteria [5]. It is believed that nanotechnological approaches in medicine will have a major impact in the next decades. Lately, controlled drug delivery systems have gained significant attention, especially with respect to the use of polymer nanofibres. Polymeric nanofibre drug delivery systems have numerous advantages over conventional dosage forms. First, the polymer can be customised to control drug-release properties. Immediate-release nanofibres can be created from water-

soluble polymers, enteric-release nanofibres can be created from enteric polymers such as methacrylic acid copolymers, and sustained-release nanofibres can be created from polylactic acid or polyvinyl acetate polymers [6]. Second, the small diameter of the nanofibres can provide a short diffusion passage, and the high surface area facilitates mass transfer and efficient drug release [7]. Third, more than one drug can be encapsulated directly into polymeric nanofibres, and these systems have shown nearly zero-order drug-release kinetics. The use of polymer nanofibres as drug carriers is therefore promising for future biomedical applications [8, 9]. For such drug delivery systems, the ability to control the length of the nanofibre is very important since the amount of drug released depends on the length of the fibre. The techniques for fabricating and chopping nanofibres that will provide the required control must therefore be developed.

1.2 Electrospinning

Electrospinning is the simplest and most cost-effective method of fabricating polymer nanofibres. This section provides an understanding of three main aspects of electrospinning. The first part explains the mechanism of electrospinning. The second describes the parameters that influence the morphology of the resultant electrospun fibres, such as the diameter and bead formation. The final part suggests a technique for fabricating and chopping nanofibres using the electrospinning process.

1.2.1 Fundamentals of electrospinning

Polymeric nanofibres can be created by means of a number of techniques, such as drawing, template synthesis, phase separation, self-assembly, and electrospinning. Of these methods, electrospinning seems to provide the simplest and most cost-effective approach for fabricating nanofibres that are uniform and controllable with respect to diameter and diversified composition [1].

Figure 1.1 is a schematic illustration of the basic setup for electrospinning. The setup has three main components: a high-voltage power supply, usually a positive or negative DC source; a spinneret that is a metallic capillary needle; and a collector that is a grounded

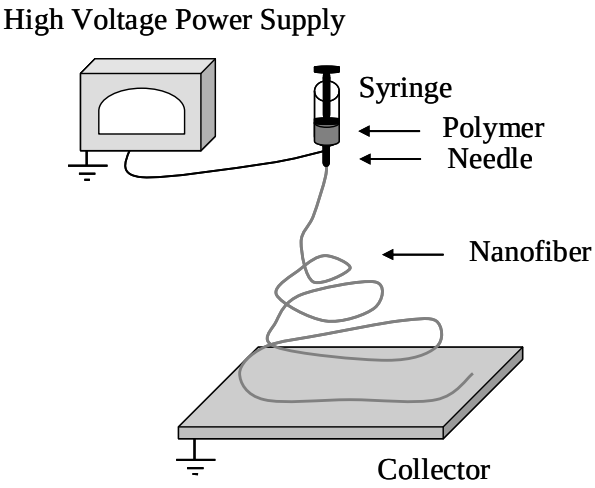

Figure 1.1: Schematic illustration of the basic setup for electrospinning

conductor. The spinneret is connected to a syringe containing the polymer solution. The syringe is placed into a syringe pump that permits the adjustment and precise control of the flow rate of the solution.

When a high voltage is applied to the spinneret, the surface of the polymer at the spinneret tip becomes electrostatically charged, and the induced charges are evenly distributed over the surface. As a result, as it is released, the droplet of solution experiences two major types of electrostatic forces. One is the Coulomb force between the surface charges. The other is the force exerted by the external electric field [4]. Under the action of these electrostatic interactions, the hemispherical surface of the solution at the tip of the capillary is distorted to form a conical shape, commonly known as a Taylor cone [10], as shown in Figure 1.2 (a). When the strength of the electric field has reached a threshold value, the electrostatic forces can overcome the surface tension of the polymer solution, and a single jet is drawn from the tip of the Taylor cone, as shown in Figure 1.2 (b). Once the jet flows away from the Taylor cone in a nearly straight line, the travelling liquid jet is subject to a variety of forces, such as the Coulomb force, the electric force imposed by the external electric field, the viscoelastic force, the surface tension force, the gravitational force, and the air drag force [1]. The result is that the bending of the jet can be observed, as shown in Figure 1.2 (c). During the process, the jet is stretched and whipped, resulting in it forming a long thread. As the liquid jet is continuously elongated and the solvent evaporates, its diameter can be greatly reduced to the nanometre scale. It is then collected on the grounded collector as a nanofibre.

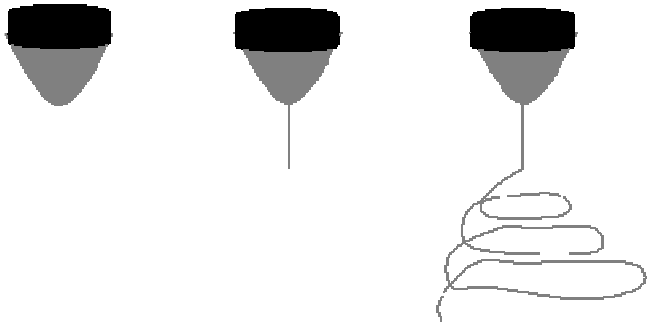

(a) (b) (c)

Figure 1.2: (a) Taylor cone (b) A single jet drawn from the Taylor cone (c) Bending instability

1.2.2 The electrospinning process

Many parameters influence the morphology of electrospun fibres, such as diameter and bead formation. These parameters can be broadly classified as polymer solution parameters, processing conditions, and ambient conditions [1].

1.2.2.1 Polymer solution parameters

The properties of the polymer solution, which include viscosity, surface tension, conductivity, and permittivity, have the significant influences on the electrospinning process and the resultant morphology.

One of the most significant parameters that influence the diameter and morphology of the fibre is the viscosity of the solution, and the element that affects the viscosity of the solution is the molecular weight of the polymer. In general, when a polymer of higher molecular weight is dissolved in a solvent, its viscosity is higher than that of a solution of the same polymer that has a lower molecular weight. Another way of increasing the viscosity of the solution is to increase the concentration of the polymer. Both using a higher molecular weight and increasing the concentration result in greater polymer chain entanglements in the solution, which is necessary for maintaining the continuity of the jet during electrospinning [1]. The polymer chain entanglements are found to have a significant impact on whether the electrospinning jet breaks up into small droplets or whether the resultant electrospun fibres contain beads [11]. Although a minimum level of viscosity is required in order to yield fibres without beads [12, 13], a viscosity that is too high will make it very difficult to pump the solution through the

syringe needle [14]. The solution may also dry at the tip of the needle before the electrospinning process can be initiated [15]. Moreover, higher viscosity results in a larger fibre diameter and smaller deposition area [1].

For electrospinning to begin, the charged solution must overcome its surface tension. At a lower viscosity, the surface tension may cause the formation of beaded fibres [1]. Lower surface tension of the spinning solution helps the onset of the electrospinning jet to occur at lower electric field.

Electrospinning involves the stretching of the solution, which is caused by the repulsion of the charges on its surface. Therefore, if the conductivity of the solution is increased, more charges can be carried by the electrospinning jet, thus resulting in the stretching of the solution. If the solution is not fully stretched, beads will form. The conductivity of the solution can be increased by the addition of ions, salt, or polyelectrolyte. An increase in conductivity also leads to a lower critical voltage for electrospinning, greater bending instability of the jet, a larger deposition area, and fibre with smaller diameters [15-17]. However, as shown in [17], there is a limit to the amount that the diameter of the fibre can be reduced.

The permittivity of a solvent has a significant influence on electrospinning. As with increased conductivity, a solution with greater permittivity produces less bead formation, greater bending instability of the jet, a larger deposition area, and fibres with smaller diameters [18-19]. The permittivity can be increased by the addition of solvents such as N,N-Dimethylformamide (DMF) [20].

1.2.2.2 Processing conditions

The parameters of the processing conditions include the voltage applied, the feed rate, the temperature of the solution, the type of collector, the diameter of the needle, and the distance between the needle tip and the collector. They influence the morphology of the fibre.

An essential element in electrospinning is the application of a high voltage to the solution. While a DC voltage supply is most commonly used in electrospinning, it is also possible to use an AC voltage for electrospinning [1]. The high voltage induces the necessary charges in the solution and the external electric field, initiates the electrospinning process when the electrostatic force in the solution overcomes the surface tension of the solution. Generally, both

a negative and a positive voltage of more than 6 kV is able to cause the drop of the solution at the tip of the needle to distort into the shape of a Taylor cone during the initiation of the jet [10]. Depending on the polymer and feed rate of the solution, a higher voltage may be required so that the Taylor cone is stable. Because both the voltage supplied and the resultant electric field have an influence on the stretching and the acceleration of the jet, they therefore also affect morphology of the fibres. In most cases, a higher voltage leads to greater stretching of the solution, resulting in a reduction in the diameter of the fibres [12, 21, 22]. In contrast, with a low voltage, closer to the critical voltage, the reduced acceleration of the jet and the weaker electric field may increase the flight time of the electrospinning jet, which may favour the formation of finer fibres [23]. With higher voltages, it has been found that the tendency for bead formation is greater [15, 24, 25], which is contrary to what would be expected, given the increased stretching of the jet due to higher voltage, which should lead to less bead formation [26].

The feed rate determines the amount of solution available for electrospinning. If a stable Taylor cone is to be maintained, each voltage has a corresponding feed rate. An increase in feed rate corresponds to an increase in the diameter of the fibre or the bead size due to a greater volume of solution leaving the needle tip [15, 27]. However, the increase in the diameter of the fibre due to a higher feed rate has an upper limit [27].

The increase of temperature causes the evaporation rate to increase and the solution viscosity to decrease. More uniform fibres have been electrospun using polyurethane at a higher temperature [23]. This may be due to the lower viscosity of the polymer solution at higher temperature. Moreover the increase in mobility of polymer molecules at higher temperature allows the Coulomb force to stretch the electrospun jet further [1].

An electric field between the high voltage at the needle and the collector is necessary for the initiation of the electrospinning. The collector plate is therefore made of a conductive material that is electrically grounded so that a stable potential difference exists between the high voltage at the needle and the collector.

The internal diameter of the needle has a specific effect on the electrospinning process. A smaller diameter has been found to reduce clogging and the numbers of beads on the electrospun fibres [28].

The flight time and the electric field strength also affect the electrospinning process and the resultant fibres. Changing the distance between the tip and the collector has a direct influence on both the flight time and the electric field strength. The electrospinning jet must be set to allow time for most of the solvents to be evaporated to form fibres. When the distance between the tip and the collector is reduced, the jet has a shorter distance to travel before it reaches the collector plate. At the same time, the electric field strength also increases, which correspondingly increases the acceleration of the jet toward the collector. As a result, there may not be enough time for the solvent to evaporate when it hits the collector [1].

1.2.2.3 Ambient conditions

The effect of the environment surrounding electrospinning jet is one area which has been still poorly investigated. The conditions involved in any interaction between the surrounding area and the polymer solution, such as humidity and pressure, may have an effect on morphology of the electrospun fibre.

Humidity may affect the polymer solution during the electrospinning. At high humidity levels, it is likely that water condenses on the surface of the fibre, resulting in a change in morphology of the fibre [12, 29]. The humidity of the environment also determines the rate of evaporation [1].

Different gases exhibit different behaviours in an electrostatic field. Thus, the composition of the air may have an effect on the electrospinning process and the morphology of the fibre [1]. A reduction in the pressure surrounding the electrospinning jet has no effect on the electrospinning process [1].

1.2.3 Chopping nanofibres with electrospinning

As mentioned in section 1.2.1, an electrified jet ejects from a Taylor cone only when the spinneret is kept at a voltage higher than the threshold value. It is therefore likely possible to chop nanofibres by controlling the applied voltage so that it is either higher or lower than the threshold, which leads to the suggested use of a high-voltage pulsed power supply.

1.3 Non-continuous-mode electrospinning

To date, no research has been conducted with respect to non-continuous-mode electrospinning that can fabricate and chop nanofibres at the same time. However, non-continuous-mode electrospraying, a technique similar to electrospinning, has been investigated. The following subsections provide the information about non-continuous-mode electrospraying, and the pulse voltages required for non-continuous-mode electrospinning.

1.3.1 Non-continuous-mode electrospraying

Non-continuous-mode electrospinning has not yet been investigated because electrospinning is still being conducted on a laboratory scale, and most researchers have focused on the diameter of the nanofibres produced rather than the length. However, the non-continuous-mode of electrospraying, which is called the drop-on-demand system, has been investigated using pulse voltage waveforms [30-33]. Electrospraying is a well-known technique that employs the same principle as electrospinning. The main difference between electrospinning and electrospraying is that the viscosity of the liquid is sufficiently low in electrospraying that the jet becomes nanoparticles rather than nanofibres [34].

The drop-on-demand system of electrospraying consists of four steps. First, a pulse voltage is applied to the spinneret where the droplets are to be prepared. Second, the applied voltage causes the meniscus of the liquid to deform into a Taylor cone, and then a jet of the liquid is ejected from the cone. Third, while the pulse voltage is off, the jet disappears, and the cone returns to the initial meniscus of the solution. Fourth, the substrate is moved to the next position where another droplet is to be prepared [32].

The influence of the value of the pulse-off voltages for pulsed electrospraying has been discussed in [30]. Figure 1.3 shows the variation in the initiation of the jet under different electrospraying potentials. Only the 2 kV potential results in an observable electrospray. Two pulse-off voltages, 0 and 1 kV, were used with a 2 kV pulse-on voltage. The results show that the 1 kV pulse-off voltage obtained a more stable pulsed electrospray than did the 0 V pulse-off voltage. When the pulse-off voltage was 0, a droplet grew up and then fell downward. This badly shaped droplet resulted in a relatively longer time to re-establish a normal Taylor cone. On the other hand, 1 kV, which was not sufficient to produce an electrospray, provided a

proper Coulomb force that could prevent the droplet from falling downward and could attract an elliptical droplet ready for the next pulsed electrospray. As a consequence, the formation time for a normal Taylor cone during the next pulse was shortened, and the pulsed electrospray eventually became much more stable. The relatively long establishing time required in the pulsed electrospray process has been experimentally tested with respect to tip geometry described.

The influence of the width of the pulse-on voltage on pulsed electrospray was discussed in [30-33]. The volume of a collected drop is proportional to the pulse-on duration minus the time delay required for a Taylor cone to form, T_{form} (approximately 3.6-5 ms) [31, 33]. The widths of the pulse-on voltages that have been used is in the range of 1-10 ms [30-33].

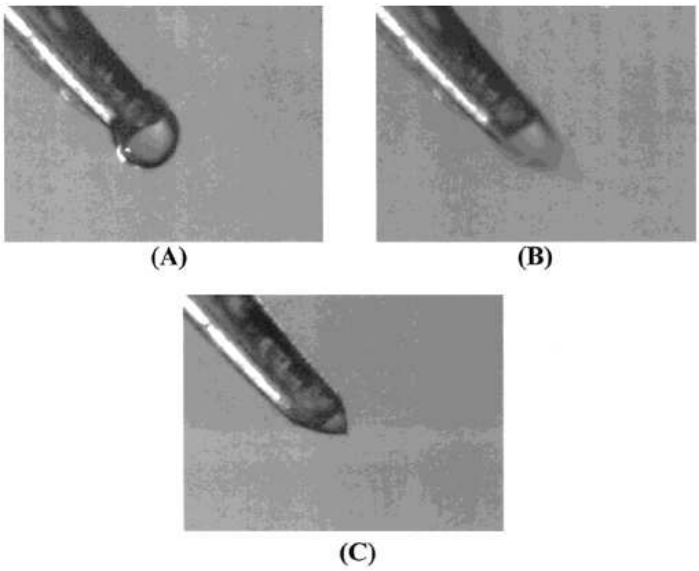

Figure 1.3: Sprayer tip and droplet at the tip under different electrospray potentials: (a) 0; (b) 1 kV; (c) 2 kV [30]

1.3.2 Pulse voltage parameters for non-continuous-mode electrospinning

Many pulse voltage parameters influence the process of non-continuous-mode electrospinning: a pulse-on voltage higher than the threshold voltage and a pulse-off voltage lower than the threshold voltage, a pulse shape, a pulse width, a time interval between pulses, and rise and fall times.

It is essential to know the threshold voltage in order to determine the pulse-on and pulse-off voltages. As mentioned in section 1.2.2.2., both high negative or positive voltages of more than 6 kV can cause the drop of solution at the tip of the needle to distort into the shape of a Taylor cone during jet initiation [10]. A DC voltage supply is most commonly used for electrospinning. Fabricating and chopping nanofibres requires the ability to control the value of the applied voltage, higher or lower than the threshold voltage as mentioned in section 1.2.3. Therefore, DC voltages at two levels is proposed: one higher than the threshold and one lower.

The time of the pulse-on voltages minus the T_{form} (section 1.3.1) determines the length of the nanofibres. An appropriate time interval between pulses is required in order that the nanofibres are chopped and that the polymer liquid is not wasted. A fast rise time is beneficial for ejecting a jet in a short period, and a fast fall time is beneficial for stopping the jet in a short period.

The key point is that the pulse voltage parameters must be highly controllable in order to produce optimal chopped nanofibres. Pulsed power supplies that can control many of the important pulse voltage parameters over a wide range and provide specific pulse shapes are therefore highly desirable.

1.4 Fundamentals of high-voltage power supplies

High-voltage pulsed power supplies are used in numerous applications, such as pulsed electrospraying, air purification, water treatment, food and liquid preservation, and radar [30-33, 35-38].

Several circuits are generally used to provide high-voltage pulses. These circuits can be divided into two groups according to their lifespan. One group that uses hard-tube gas

discharge switches such as a thyratron has a limited lifespan. The other group uses semiconductor switches and has a semi-infinite lifespan [39]. A conventional high-voltage pulse power supply uses a hard-tube switch because of its high-voltage capabilities and fast turn-on times. However, with a thyratron switch, only the turn-on time is controllable, leaving the turn-off time dependent on the RC time constant of the load resistance and the energy storage capacitor, leading to an exponential decay pulse. Square pulses are more desirable than exponential for controlling the length of the nanofibres. Advances in semiconductor switches have led to devices with higher voltages and current ratings. Although the voltage ratings of semiconductor devices are not as high as those of hard-tube devices, they can be stacked in series to obtain the required voltage ratings. Because semiconductor switches have controllable turn-on and turn-off times, they can produce square pulses with controllable widths. Semiconductor switches also have the advantage of high repetition rates. For this reason, a recent trend has been to use power semiconductor devices such as bipolar junction transistors (BJTs), metal oxide semiconductor field effect transistors (MOSFETs), gate turn off (GTO) thyristors, and insulated gate bipolar transistors (IGBTs) for high-voltage pulsed power supplies [40, 41].

Table 1.1 shows the comparison of controllable semiconductors. IGBTs have some of the advantages of MOSFETs, BJTs, and GTOs combined. Similar to MOSFETs, the IGBTs have high-impedance gates, which require only a small amount of energy to switch the devices. Like BJTs, IGBTs have small on-state voltages even in devices with large blocking voltage ratings. Similar to GTOs, IGBTs can be designed to block negative voltages [41]. Therefore, IGBTs are preferable for this research due to these advantages.

Discrete IGBTs are available up to 6.5 kV, the turn-on and turn-off times of which are measured at ~180 ns and ~5 μs, respectively [42]. This time is short enough for the application investigated in this research. In terms of cost, the 6.5 kV IGBTs are more expensive since only IGBTs with a high-current rating (200 A) are currently available [43]. On the other hand, reasonably priced 4 kV IGBTs are available with medium current ratings (30 A) [44]. Therefore, it is more reasonable to use several IGBTs in series to increase the voltage capabilities of the device if a high-current rating is not required. The use of lower voltage-rated IGBTs in series also results in improved turn-on and turn-off times compared with the use of a high-rating IGBT [42].

Table 1.1: Relative properties of controllable switches [41]

Device	Power capability	Switching speed
BJT	Medium	Medium
MOSFET	Low	Fast
GTO	High	Slow
IGBT	Medium	Medium

There are two major criteria for connecting semiconductor switches in series. First, series switches should turn on and off at the same time; otherwise, at turn-on, the slowest device takes the full voltage and may be damaged. Similarly, at turn-off, the fastest switch takes the full voltage and may be damaged. The characteristics of switches with the same part number vary significantly due to the manufacturing process. By nature, switches do not turn on and off at the same time, even if simultaneous gating signals are applied to all of them [45]. Therefore, using fewer IGBTs leads to less chance of bad synchronization of their commutation. Second, series switches should take approximately the same share of the total voltage. External elements are used to equalize voltage sharing among series switches in steady-state as well as during turn-on and turn-off transients [45].

1.5 Aim of the present work and thesis organization

Nanofibres have been the subject of recent intensive research because of their unique properties, especially their huge surface-area-to-volume ratio, which is about one thousand times higher than that of a human hair. Many studies have therefore been published on the subject of electrospinning for fabricating nanofibres. However, no research has examined non-continuous-mode electrospinning.

This work has two main objectives: designing a high-voltage pulsed power supply and applying it for non-continuous-mode electrospinning in order to fabricate and chop polymer nanofibres.

The more specific objectives of the thesis are as follows:

- To design an IGBT-based pulsed power supply capable of producing square pulses with amplitudes up to 10 kV and widths of microseconds.
- To provide a high degree of control of the pulse amplitude, pulse width, number of pulses, and time between pulses.

- To apply the pulsed power that are designed and built as part of this research in order to investigate non-continuous-mode electrospinning.

The thesis is organized as follows:

- Chapter 2 consists of two main sections, the first of which describes the design and construction of the IGBT-based pulsed power supply. Each element, power and control module, IGBT driver, optocoupler, and series-connected IGBTs is explained. The requirement for the external circuits for voltage sharing among series-connected IGBTs and an external shaping resistor are also presented. The second section describes the materials and the experimental apparatus for electrospinning that have been used in this research.
- Chapter 3 is divided into two sections. The first section presents the evaluation of the pulsed pulse supply that is used for non-continuous-mode electrospinning. The effect of varying the load resistance on the pulse voltage and the pulse width is investigated. Also, the voltage distribution in the series-connected IGBTs is presented. In addition, the determination of the pulse-on and pulse-off voltages is explained. The second section presents the investigation of non-continuous-mode electrospinning using a polyethylene oxide (PEO) solution and alginate/PEO solutions.
- Chapter 4 provides the analysis and discussion of the results presented in the previous chapter. This enables the important factors that influence the pulse parameters of the pulse voltage and the non-continuous-mode electrospinning to be indentified. These results are explained in detail and, whenever possible, compared to similar results reported in the literature.
- Chapter 5 is a summary of this thesis and provides some suggestion for future work.

Chapter 2

Experimental setup

This chapter provides the information necessary for an understanding of the IGBT-based pulsed power supply that has been designed and built for electrospinning to fabricate and chop nanofibres. Also, this chapter describes the polymers used in this study and the experimental apparatus for electrospinning.

2.1 Design of the pulsed power supply

This section explains the design and construction of the modules of the IGBT-based pulsed power supply. The modules include the power and control module, IGBT driver and optocoupler, series-connected IGBTs and external circuits for voltage sharing among series-connected IGBTs, and an external wave shaping resistor.

2.1.1 Power and control module

The power module enables the pulsed power supply to be connected to and to be powered from a standard 110 V electrical outlet. This feature increases flexibility of the module so that the pulsed power supply can function in any laboratory. The module also has 9 V DC batteries that are needed to power both a timer and three IGBT driver circuits. It contains a timer that replaces the function generator that is used to vary the width of the pulses and the number of pulses per second.

2.1.1.1 Power supplies

To function properly, the timer and the three IGBT drivers require 9 V DC batteries, a battery for the timer and two batteries for each IGBT driver. Batteries are used rather than external DC source so that there is no need to use additional isolation transformers as the control module floats at high voltage, which makes the module more compact and reasonably priced. The external source needed for the pulsed power supply is a high-voltage DC source,

which is used to produce the desired pulsed output voltage by switching the IGBTs on and off. For the purpose of this research, an SH030R270 (30 kV and 270 mA) high-voltage DC source manufactured by Glassman High-voltage, Inc. was used.

2.1.1.2 Trigger circuit

A precise control of the pulse parameters is important for non-continuous-mode electrospinning, especially when it is necessary to optimize this process. For this reason, the LM555 timer IC, manufactured by National Semiconductor, was chosen for sending a signal to the IGBT driver circuits. The LM555 is a simple, yet versatile, device, which is highly stable for generating accurate time delays or oscillation.

For the astable operation of the LM555, the free running frequency and duty cycle are accurately controlled by two external resistors and a capacitor. Figure 2.1 shows the trigger circuit for the astable operation of the LM555. In this operation, the capacitor charges and discharges between 1/3 Vcc and 2/3 Vcc. As in the triggered mode, the charging and discharging times, and therefore, the frequency are independent of the supply voltage. The following formulas were used to determine the frequency, pulse width, and duty ratio [46].

The charging time (output high) is given by

$$t_1 = 0.693(R_A + R_B)C \tag{2.1}$$

And the discharging time (output low) by

$$t_2 = 0.693(R_B)C \tag{2.2}$$

Thus, the total period is

$$T = t_1 + t_2 = 0.693(R_A + R_B)C = 1/f \tag{2.3}$$

The duty ratio is

$$D = R_B/(R_A + 2R_B) \tag{2.4}$$

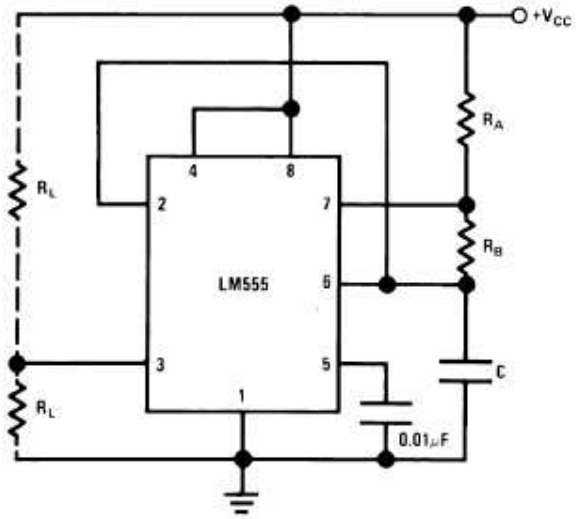

Figure 2.1: Trigger circuit for the astable operation of LM555 [46]

For the purposes of non-continuous-mode electrospinning, a signal of T=0.1-1 s and D=20-40 % are required as discussed later. Thus, R_A=2 Ω-1 MΩ, R_B=1-100 kΩ, and C=10 μF can be obtained and used after substituting T=0.1-1 s and D=10-50 % into equations (2.3) and (2.4). One of the characteristics of the LM555 in astable mode is that the pulse width of the on-state is longer than that of the off-state. However, the pulse width of the on-state should be shorter than that of the off-state for this research. To achieve this effect, a TLC2272A amplifier manufactured by Texas Instruments, was connected to the LM555 as an inverter. The LM555 was used to trigger multiple IGBTs in series in order to reduce the cost, the number of components, and the complexity of the synchronization of the turn on and turn off of the IGBTs. The output power from the LM555 is not strong enough to provide trigger signals to three IGBTs; hence, the TLC2272As were used to amplify the output power. A photograph and schematic of the trigger circuit are shown in Figures 2.2 and 2.3, respectively.

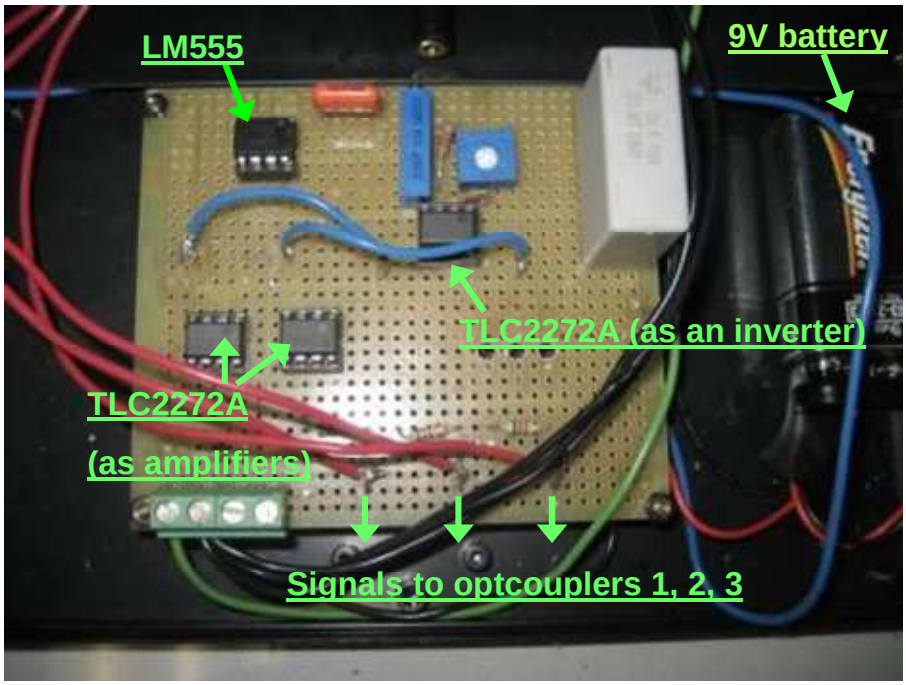

Figure 2.2: Photograph of the trigger circuit

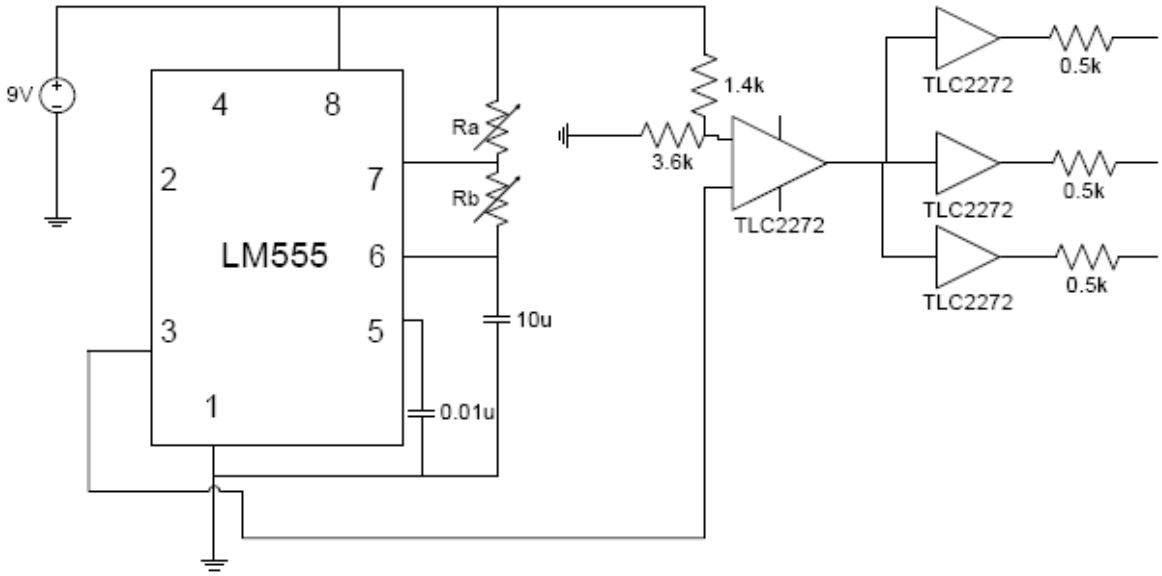

Figure 2.3: Schematic of the trigger circuit

2.1.2 IGBT, IGBT driver, and optocoupler

The ideal IGBT for this research would be able to withstand a high collector-emitter voltage. As mentioned in section 1.4, it is more reasonable to use several IGBTs in series to increase the voltage capability. Based on this criterion, the IGBTs that were chosen for the design and construction of the pulsed power supply for this research were the IXGF30N400 switches, manufactured by IXYS. This IGBT has a collector-emitter breakdown voltage of 4 kV and a current rating of 30 A. The IXGF30N400 has an input capacitance of 3040 pF that must be charged and discharged in order to turn the IGBT on and off. The LM555 is not capable of fully and rapidly charging and discharging the input capacitors of the IGBTs; therefore IGBT drivers were used.

The ability of the IGBT driver circuit to charge the input capacitor of the IGBT determines its switching behaviour and power dissipation. The driver should have small output impedance so that its current driving capability is large enough to rapidly charge the input capacitors. Therefore, the TD351 chips, manufactured by STMicroelectronics, were used as the IGBT driver for the IXGF30N400. Electrical isolation between the trigger circuit and the driver circuit is required in order to prevent the LM555 from high voltage damage because it operates from a 9 V battery but is used to control IGBT's switching at a high-voltage level of 10 kV. The reasons for operating the electrospinning setup at 10 kV are explained in section 3.1.3.

The simple way to provide electrical isolation is to use optocouplers. An optocoupler provides an optical link between the low-voltage side and the high-voltage side, which is isolated electrically from the low voltage. Because the IGBTs operate at 10 kV, the isolation of the optocouplers should be higher than 10 kV. Based on this criterion, the optocouplers used for this research were the OPI1268, manufactured by OPTEK Technology Inc. The OPI1268 is a 16 kV isolator with a digital output capable of high-speed data transmission.

The 9 V batteries and the LM555 that are part of the power and control module, along with the rest of the circuit, were built as close to the IGBTs as possible in order to minimize stray inductance of the wire. Both the OPI1268 and the TD351 are inverters ICs. The TLC2272A inverter was connected to the LM555. The high output of the IGBT drivers produced by the low output of the LM555 is thus at potentials of 9 V. This 9 V potential charges the input capacitances of the IGBTs, and they are turned on as a result. On the other hand, the low output of the IGBT drivers produced by the high output of the LM555 is at -9 V, resulting in

the IGBT turn off. The photograph of the IGBT driver and optocoupler is shown in Figure 2.4. A schematic of series-connected IGBTs, IGBT drivers, and optocouplers is shown in Figure 2.5.

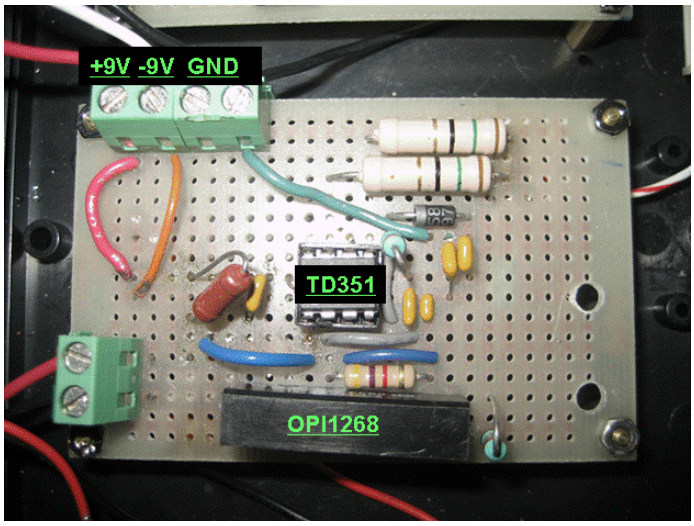

Figure 2.4: Photograph of the IGBT driver and optocoupler

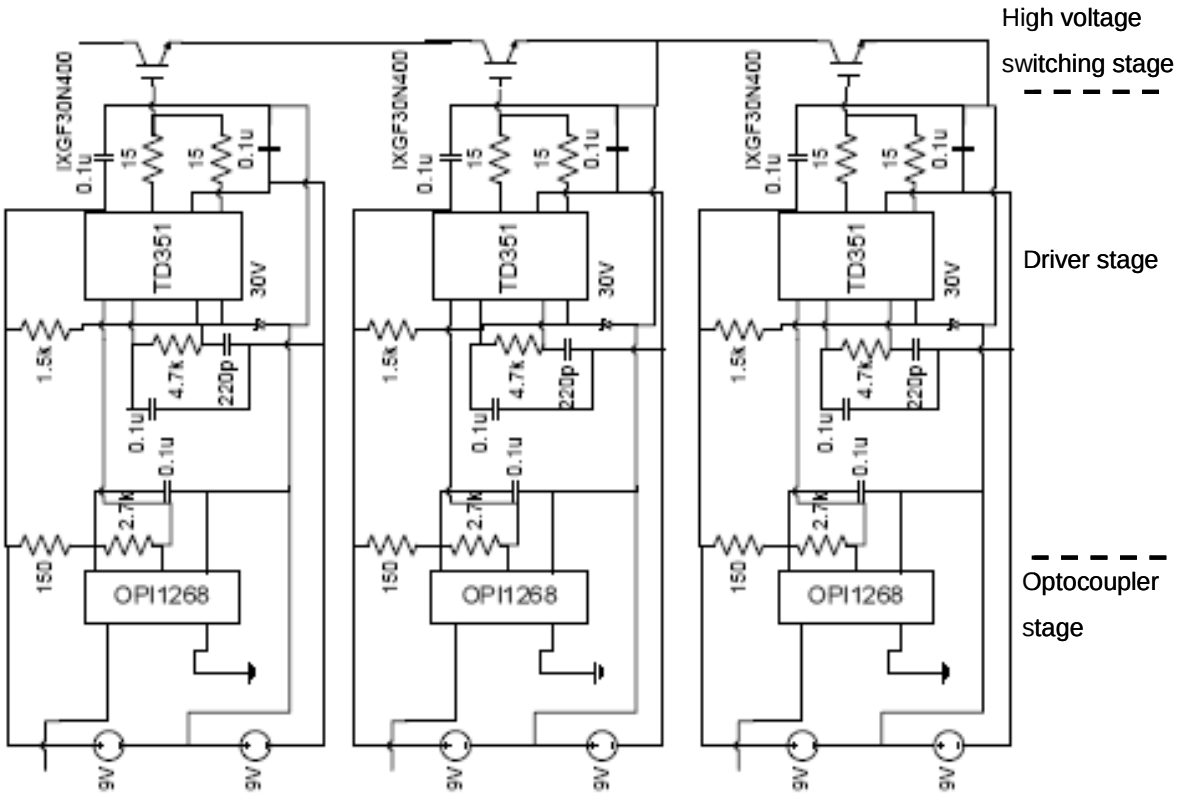

Figure 2.5: Schematic of the series-connected IGBTs, IGBT drivers, and optcouplers

2.1.3 Series-connected IGBTs and the external circuits for voltage sharing

An applied voltage of at least 10 kV is required for non-continuous-mode electrospinning. It is necessary to use several IGBTs in series in order to increase the voltage capability. Connecting three identical IGBTs in series allows the total voltage to be three times the rating of one IGBT. Each IGBT requires an IGBT driver as can be seen in Figure 2.5. As mentioned in section 2.1.1.2, one trigger circuit was used in order to provide trigger signals for all IGBTs.

IGBTs connected in series have two major requirements. First, series IGBTs should turn on and turn off at the same time in order to avoid poor synchronization. Using a fewer IGBTs therefore leads to a fewer chances of poor synchronization of their commutation. To meet this requirement, only three IGBTs were connected in series for this application.

Second, external elements should be used to equalize the voltage sharing among the IGBTs connected in series at steady-state as well as during turn-on and turn-off transients. At off-state, an IGBT can be represented by its blocking resistance. Because blocking resistances vary, the voltage sharing among the switches is uneven, which can cause damage to the IGBTs because an IGBT might be subject to a higher voltage that it can withstand. To mitigate this effect, a resistor should be placed across every IGBT so that the total voltage is shared equally. To determine the value of the resistor $R_{steady\text{-}state,}$ the load resistance R_{load} must be considered. The R_{load}, which in an electrospinning setup is in parallel with a wave shaping resistor, 1 MΩ as discussed in section 2.1.4. If the value of $R_{steady\text{-}state}$ is too small compared with that of R_{load}, the most of the voltage appears on the R_{load} even during off-state. It is therefore important to keep a balance between the value of $R_{steady\text{-}state}$ and R_{load}. For this research, these factor were considered, $R_{steady\text{-}state}$ was determined to be 1 MΩ. During on-state, only the R_{load} is taken into account; hence, all of the 10 kV applied voltage appears only on R_{load} and no voltage appears on $R_{steady\text{-}state}$. The reverse conditions apply during off-state, and the three values of $R_{steady\text{-}state}$ and R_{load} were considered with respect that 2.5 kV appears on each $R_{steady\text{-}state}$ and R_{load}. The $R_{steady\text{-}state}$ thus makes the voltage sharing possible equally during steady-state.

To facilitate voltage sharing during turn-on and turn-off transients, a snubber circuit must be connected to each IGBT. In general, a snubber circuit is used to control dv/dt and di/dt across devices. However, the structure of voltage sharing during transients is the same as that

of dv/dt snubber circuit. If the current and voltage transitions during the turn-on and turn-off processes are assumed to be linear, stray inductances to be negligible, no overshoot and undershoot are observed in the current and voltage-switching waveforms. However, in a real-life situation, stray inductances cannot be neglected. As a result, overshoots and undershoots in the voltage and current switching waveforms can be observed. To reduce the overshoots, snubber circuits are used across the switches. In general, an RC circuit is used across each of the series-connected switches. Figure 2.6 shows the RC circuit which was used for the IGBTs in this study. The capacitor placed across the switch opposes sudden changes in the voltage and ensures an even distribution of voltage among the series switches during transients. Almost all of the energy stored in the capacitor is dissipated in R, with almost no dissipation in the switch. The RC snubber circuit was designed as follows [45]. Equation (2.5) was used to determine the capacitance value with a safety factor of 1.5 to dv/dt [45].

$$C_S = \frac{1.5 I_0 t_{fi}}{2 V_d} \tag{2.5}$$

In this research, the load resistor, R_{load}, is 1 MΩ and the applied voltage is 10 kV. Thus, I_0 is calculated to be $I_0 = V_{applied} / R_{load} = 10 \text{ kV} / 1 \text{ M}\Omega = 10 \text{ mA}$. From the data sheet of the IXGF30N400, t_{fi} is 514 ns. V_d is the voltage applied to each IGBT, which is, approximately 3.3 kV. After these values are substituted into equation (2.5), *Cs* is calculated to be 1.168 pF. *Cs* has to larger than 1.168 pF; hence, 20 pF was used here. For *Rs*, equation (2.6) was used to determine the resistor value.

$$I_0 + \frac{V_d}{R_{s,\min}} = I_{DM} \tag{2.6}$$

I_{DM} is given to be 30 A from the IXGF30N400 data sheet. I_0 and V_d are the same as used in equation (2.5). Therefore, $R_{s,\,min}$ is calculated to be 110 Ω. The resistance has to be larger than $R_{s,\,min}$; hence, 150 Ω was used as R_s.

A photograph and a schematic of the IGBTs and the external circuit for voltage sharing are shown in Figures 2.7 and 2.8, respectively.

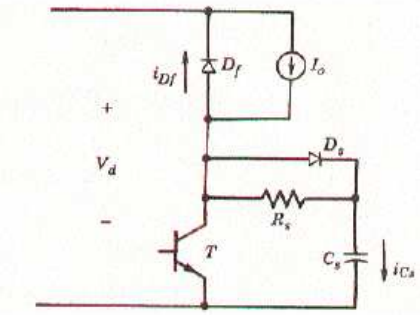

Figure 2.6: RC snubber circuit [45]

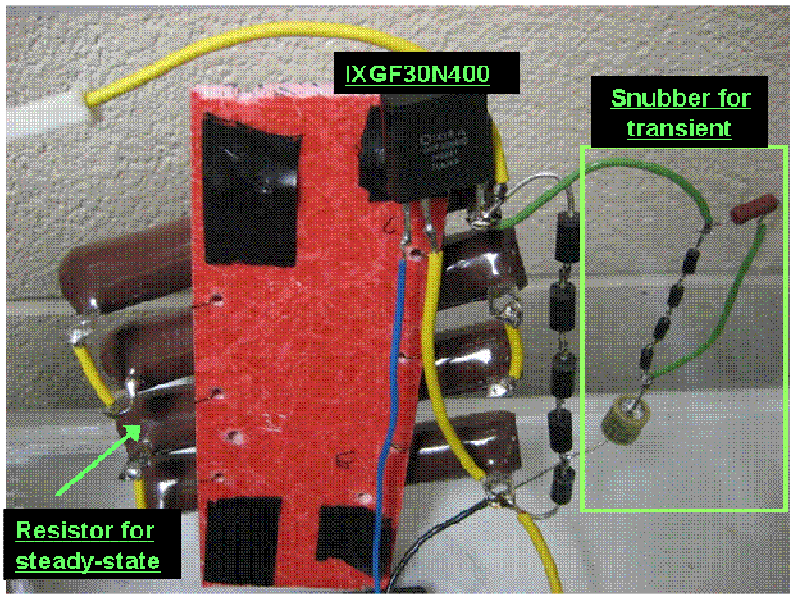

Figure 2.7: Photograph of the IGBT and the circuit for voltage sharing

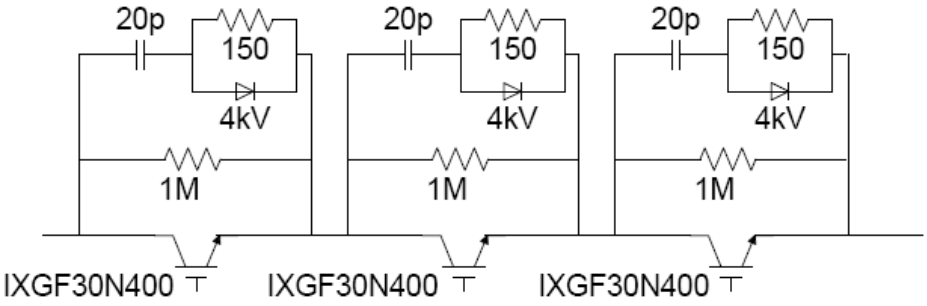

Figure 2.8: Schematic of the series-connected IGBTs and the external circuits for voltage sharing

2.1.4 External wave shaping resistor

Transistors act as switches with two conducting states, on and off, depending on the gate terminal voltage. An ideal transistor has zero resistance when it is in the on state and infinite resistance during the off state. However, in practice, transistors are not ideal switches. IGBTs have a small resistance in their conducting state and a high but not infinite resistance in the off state [47]. In addition, a 1 MΩ $R_{steady\text{-}state}$ has been connected to each IGBT in order to share the voltage equally during steady-state, as mentioned in section 2.1.3. Therefore, if the load connected to the end of the pulse circuit is relatively large compared to $R_{steady\text{-}state,}$ most of the voltage appears at the load even when the IGBTs are turned off. A pulse circuit was simulated in order to investigate the output voltage at the load.

The above pulse circuit was simulated using PSIM software, manufactured by Powersim Inc. Figures 2.9 and 2.10 show the pulse circuit with the electrospinning setup and the simulation result of the output voltage across the 500 MΩ load, respectively. In Figure 2.9, the 500 MΩ load connected to the pulse circuit is the approximate resistance of the electrospinning setup that has been used.

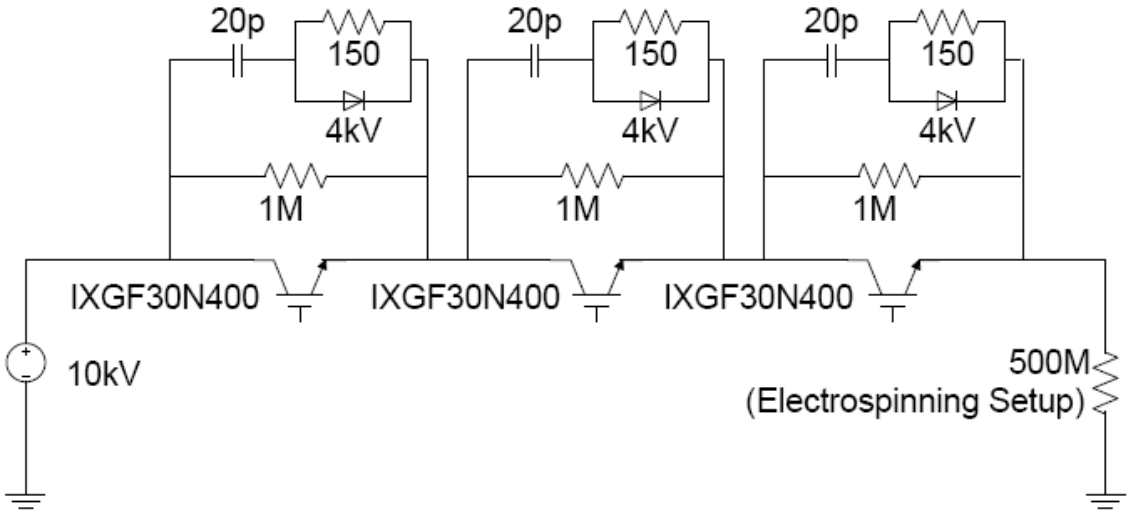

Figure 2.9: Schematic of the pulse circuit with the electrospinning setup as load

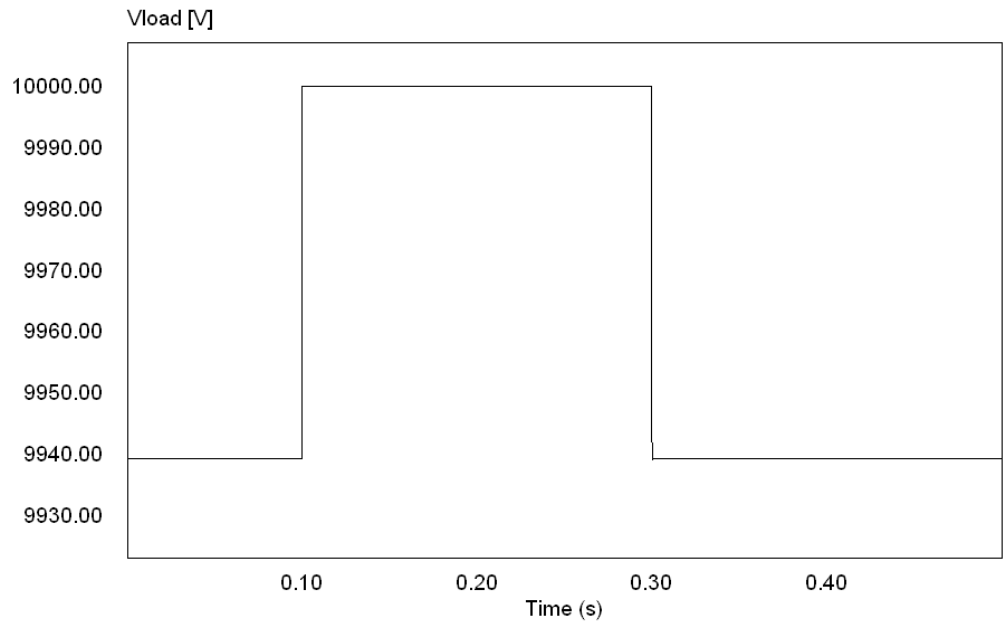

Figure 2.10: Simulation result of the output voltage across the 500 MΩ load

As can be seen in Figure 2.10, the off-pulse voltage across the 500 MΩ load stays close to 10 kV because the 500 MΩ is relatively large compared with $R_{steady\text{-}state}$. To stop a jet from a needle for non-continuous-mode electrospinning, the off-pulse voltage should be below 3 kV as is discussed in section 3.2.1. To solve this problem, the value of the load must be decreased. Therefore, an external 1 MΩ wave shaping resistor was connected to the 500MΩ load in parallel. Figures 2.11 and 2.12 show the pulse circuit with the electrospinning setup in parallel with the external shaping resistor and the simulation result of the output voltage across the 500 MΩ and 1 MΩ loads connected in parallel, respectively. As can be seen in Figure 2.12, the pulse-off voltage drops to 2.5 kV after an external shaping resistor is added.

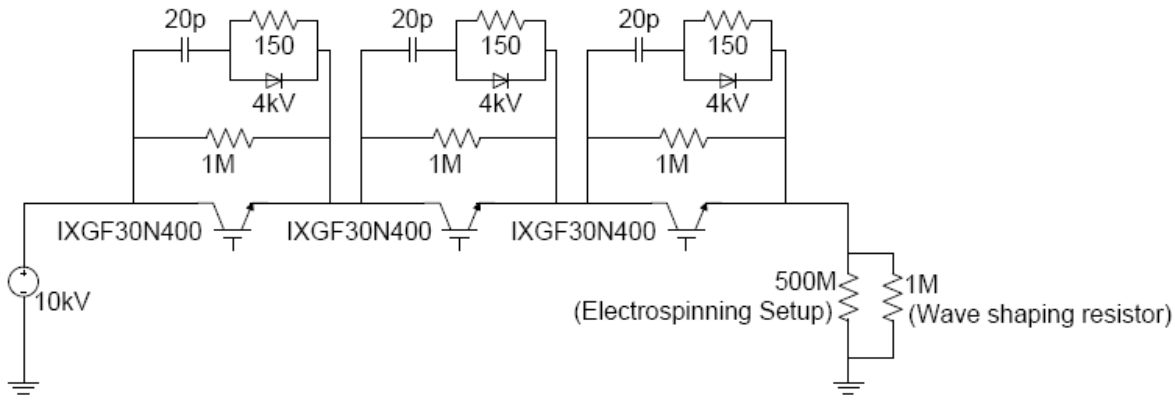

Figure 2.11: Schematic of the pulse circuit with the electrospinning setup in parallel with the external wave shaping resistor

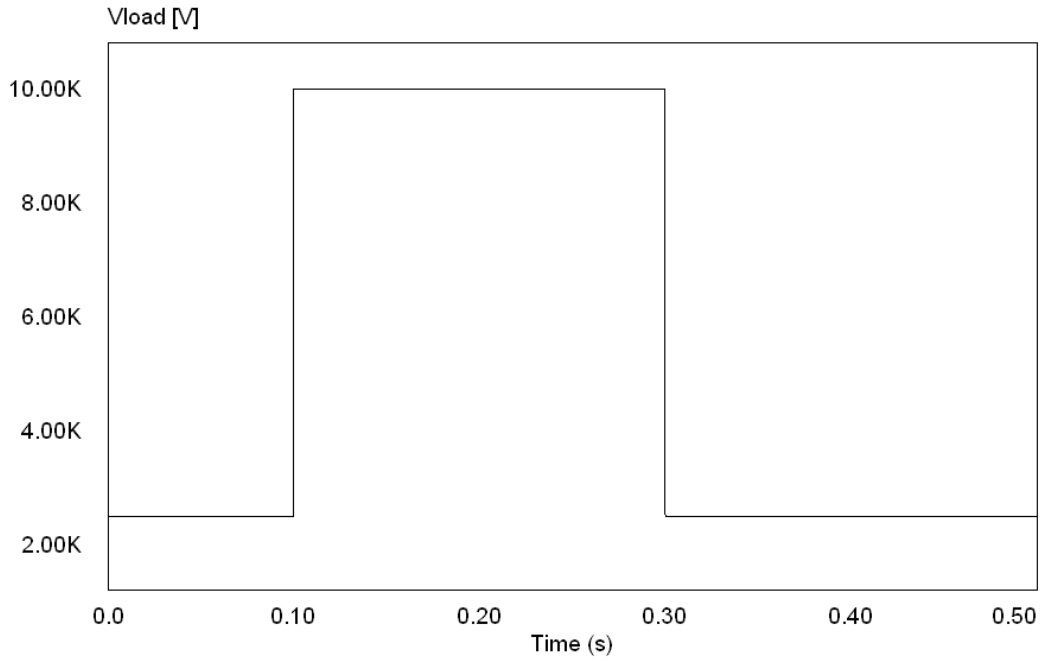

Figure 2.12: Simulation result of the output voltage across the 500 MΩ and 1 MΩ loads connected in parallel

2.2 Materials and electrospinning apparatus

Many kinds of polymers have already been successfully electrospun. Also, various kinds of electrospinning apparatus have been used. Two polymers were chosen for the preparation of the solutions, Polyethylene oxide (PEO) and alginate, in this study. The electrospinning apparatus that has been used for this research is also described in 2.2.2.

2.2.1 Materials

To date, over 50 synthetic or natural polymers and polymer blends have been successfully spun using the electrospinning process, for the most part in research laboratories [48]. Polymers consist of a long chain of molecules with repeating units called monomers that are generally covalently bonded to one another. Polymers exhibit several properties that are attractive for many applications, and specific material properties must be considered depending on the type of application. The current research initially employed PEO, which is synthetic polymer, several blends of which have been used for diverse applications in recent studies[1]. PEO is easy to spin; hence, it helps to evaluate the system of electrospinning. For biomedical applications such as drug delivery, the materials used must be biocompatible, and natural polymers are therefore preferable [1, 49]. For these reasons, PEO, a synthetic polymer, and alginate, a natural polymer, have been used in this research.

2.2.1.1 Polyethylene oxide

PEO is a synthetic polymer that contains only a single type of monomer known as a homopolymer. The electrospinning of PEO is well investigated and understood. The PEO fibres produced by electrospinning often exhibit good mechanical properties, and the inherently hydrophilic surface suppresses non-specific adsorption of polypeptides that might be important for the accessibility, as well as the biofunction, of surface-tethered polypeptides. The intrinsic crystallinity of PEO is responsible for the formation of physically crosslinked domains that not only contribute to fibre stability but also prevent the reverse diffusion of surface polypeptide back into the interior of the hydrophilic fibre. In addition to these advantages, well-defined PEO is commercially available in a broad range of molecular weights and is

generally approved for biomaterial fabrication. These attributes make PEO an ideal model system with which to establish reliable procedures for fibre preparation, analysis, and perhaps even biological testing [49]. For these reasons, PEO with a molecular weight of 600,000, purchased from Aldrich Co., was chosen for the preparation of the solution for electrospinning. The PEO fibres were electrospun using a 5 % (w/w) concentration of PEO in distilled water.

2.2.1.2 Alginate

One of the greatest potentials for electrospun fibre is in the area of bioengineering. For many biomedical applications, the materials used must be biocompatible, and natural polymers thus have a distinct advantage over synthetic materials. Since most natural polymers can be degraded by naturally occurring enzymes, they can be used in applications where temporary implants are desired or for drug release. It is also possible to control the degradation rate of the implanted or drug release polymer by chemical cross-linking or other chemical modifications, thus allowing greater versatility in the design of the implant and drug release mechanism [50]. One of natural polymers is alginate.

Alginate, a polysaccharide derived from brown seaweed [51], is biodegradable, has controllable porosity, and may be linked to other biologically active molecules [52, 53]. Electrospinning of the alginate from aqueous solutions seems difficult. The repulsive force among the polyanions could be the reason hindering electrospinning of sodium alginate. In fact the alginate has been successful in polymer blends formed by blending the alginate with a non-toxic, non-ionic, and biocompatible synthetic polymer such as PEO. The conductivity of a 2 % solution of sodium alginate is reduced by 16 % after adding half the amount of PEO, which indicates the reduction of the repulsive force among polyanionic sodium alginate molecules. The reduction allows successful electrospinning of the sodium alginate and PEO blends [54].

Based on the above discussion, an alginate solution blended with PEO was selected for electrospinning. Sodium alginate from brown algae (2500 cps and a 2 % solution at 25 °C) and PEO with a molecular weight of 900,000 were chosen for the preparation of the blended solution. Alginate and PEO solutions with a 3 % (w/w) concentration in distilled water were first prepared separately. Then, the alginate and PEO solutions were blended together.

2.2.2 Electrospinning apparatus

Figure 2.13 is a schematic of the experimental setup used to perform the electrospinning experiments. It consists of a high-voltage power supply, a pulse circuit, a wave shaping resistor, a syringe pump, a syringe, a polymer solution, a metallic needle, and a grounded collector. A Glassman DC supply was used to apply a high voltage, positive 10 kV, connected to the pulse circuit. A wave shaping resistor was connected to the electrospinning setup in parallel. The pulse voltage was applied between the needle and the collector plate. The polymer solution was forced through a syringe needle at a constant rate of 0.04 ml/min by the syringe pump, resulting in the formation of a droplet of polymer solution at the syringe tip. An AWG 24 blunt needle was used with the syringe that was placed vertically above the collector plate during all the experiments. The electrospun fibres were collected on a grounded collector that is a thin round plate made of aluminum, with a diameter of 300 mm. Then, a Leo 1530 Germini scanning electron microscope (SEM) was used to see the morphology of the electrospun fibres. Figure 2.14 shows the photograph of the experimental setup that has been used.

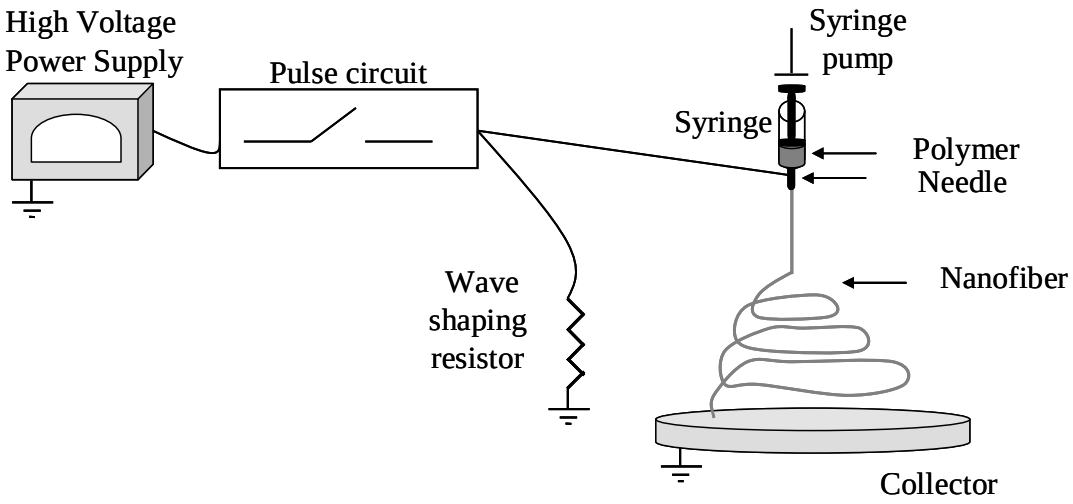

Figure 2.13: Schematic of the actual experimental setup for electrospinning

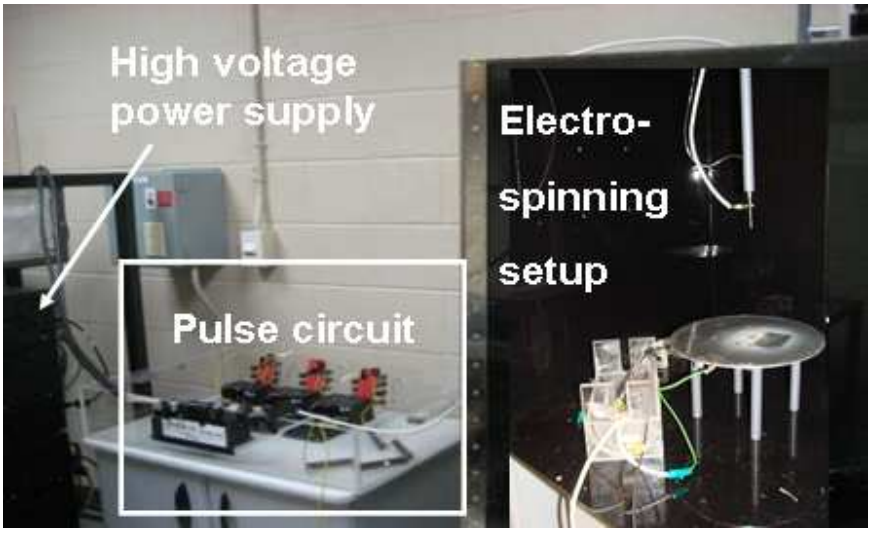

Figure 2.14: Photograph of the actual experimental setup for electrospinning

Chapter 3

Results

This chapter is divided into two sections. The first section presents the evaluation of the pulsed power supply that is used for non-continuous-mode electrospinning. The second part, presents the investigation of non-continuous-mode electrospinning using a PEO solution and alginate/PEO solutions.

3.1 Evaluations of the pulsed power supply

This section presents the effects on the output voltage produced by the single IGBT and the series-connected IGBT pulsed power supplies when the load resistances are varied. The load resistance was varied in order to determine its effect on the pulse-on and pulse-off voltages and the pulse width. The voltage distribution of each IGBT in the series-connected IGBTs was also measured in order to ensure that the voltage is below the voltage rating of the IXGF30N400. The last subsection explains how the pulse-on and pulse-off voltages that are applied for non-continuous-mode electrospinning were determined based on the results of the electrified jets produced with DC voltage. In all of the experiments, the output voltage pulses were measured using a Tektronix P6015A 1000x high-voltage probe, and a Le Croy Corp. WaveJet 312 oscilloscope. The rise and fall times of the output voltages were recorded using the 10 % and 90 % of the full voltage of the pulse. The oscilloscope measured the pulse width at the full width at half maximum (FWHM), which is the width at the middle of the pulse.

3.1.1 Single IGBT

The characteristics of the single IGBT, IXGF30N400, were investigated before the series-connected IGBT pulsed power supply was tested. The single IGBT was tested under three different conditions with varying resistive loads: the IGBT, the IGBT with the circuit for voltage sharing during transient, and the IGBT with the circuit for voltage sharing during transient and steady-state. Figure 3.1 shows the IGBTs under the three different conditions and

the test circuit for each. Figure 3.2 shows sample output voltages produced for case 2 when R_{load} is 1 MΩ.

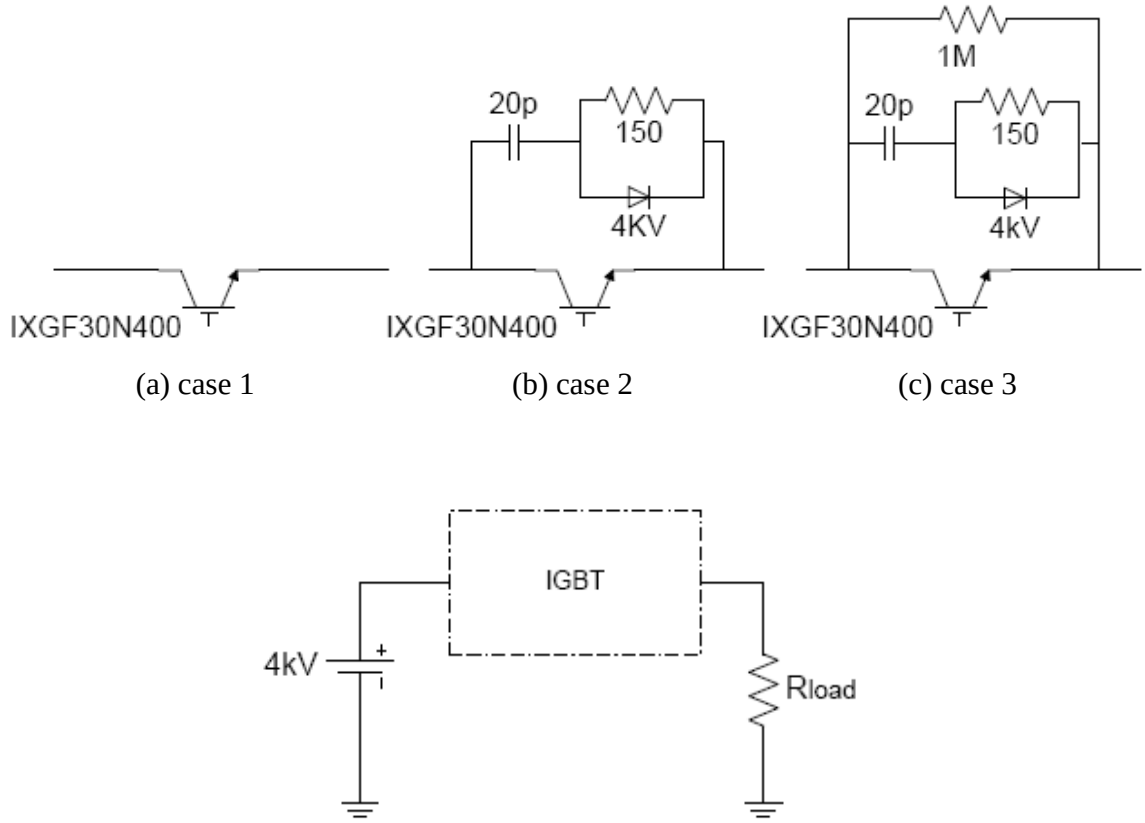

(a) case 1 (b) case 2 (c) case 3

(d)

Figure 3.1: Single IGBT test conditions: (a) Case 1: IGBT (b) Case 2: IGBT with the circuit for voltage sharing during transient (c) Case 3: IGBT with the circuit for voltage sharing during transient and steady-state (d) Test circuit

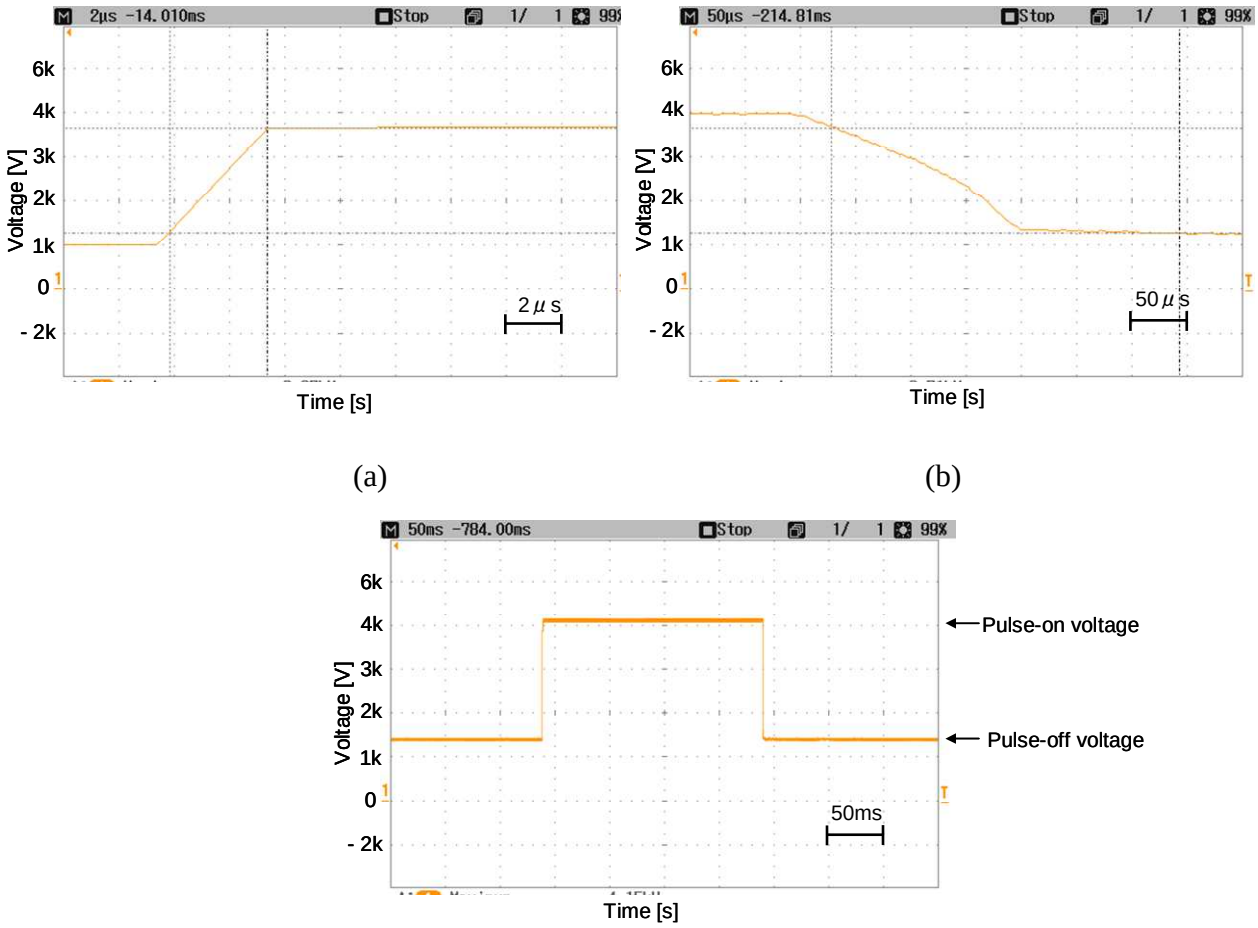

(a) (b)

(c)

Figure 3.2: Measured output voltage waveform produced by the single IGBT with the external circuit for voltage sharing during transient when R_{load} is 1 MΩ: (a) pulse rise time (b) pulse fall time (c) a complete pulse waveform

3.1.1.1 Effect on the pulse-on and pulse-off voltages

The pulse-on and pulse-off voltages are important parameters for non-continuous-mode electrospinning. To start a jet, the pulse-on voltage should be above the threshold. The pulse-on voltage also affects the morphology of the nanofibres, such as the diameter and the bead formation. To stop the jet, the pulse-off voltage should be below the threshold voltage. The pulse-on and pulse-off voltages across the R_{load} shown in Figure 3.1 were measured by varying the value of the R_{load}. The change in the R_{load} affected the pulse-on and pulse-off voltages.

Figures 3.3 and 3.4 illustrate the effects of varying the R_{load} on the pulse-on and pulse-off voltages for cases 1, 2 and 3 illustrated in Figure 3.1. As indicated in Figure 3.3, an increase in the R_{load} results in a small or no change in the pulse-on voltage for cases 1, 2 and 3. On the other hand, as shown in Figure 3.4, an increase in the R_{load} results in an increase in the pulse-off voltage for cases 1, 2 and 3. When case 3 is compared with cases 1 and 2, the rate of change in the pulse-off voltage becomes greater as the R_{load} increases. Although the values for case 1 and 2 are different, they have a similar tendency with respect to the rate of change. When the R_{load} was changed from 500 kΩ to 1500 kΩ, the pulse-off voltage increased by 119 % in case 1, 127 % in case 2, and 157 % in case 3.

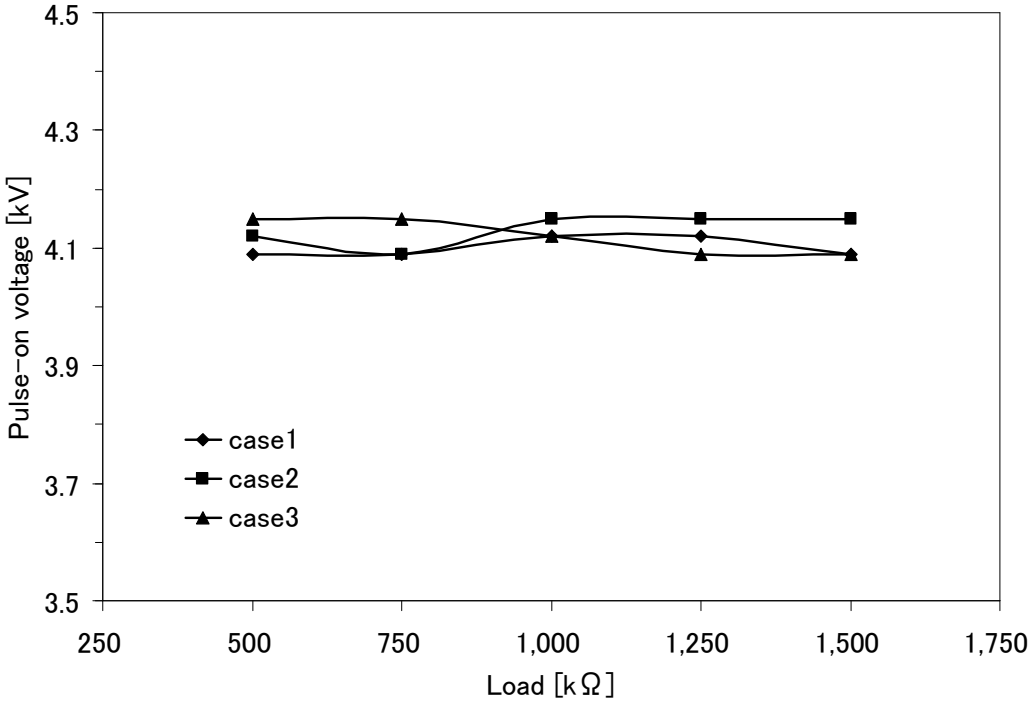

Figure 3.3: Measured pulse-on voltage versus R_{load} for cases 1, 2, and 3 in Figure 3.1

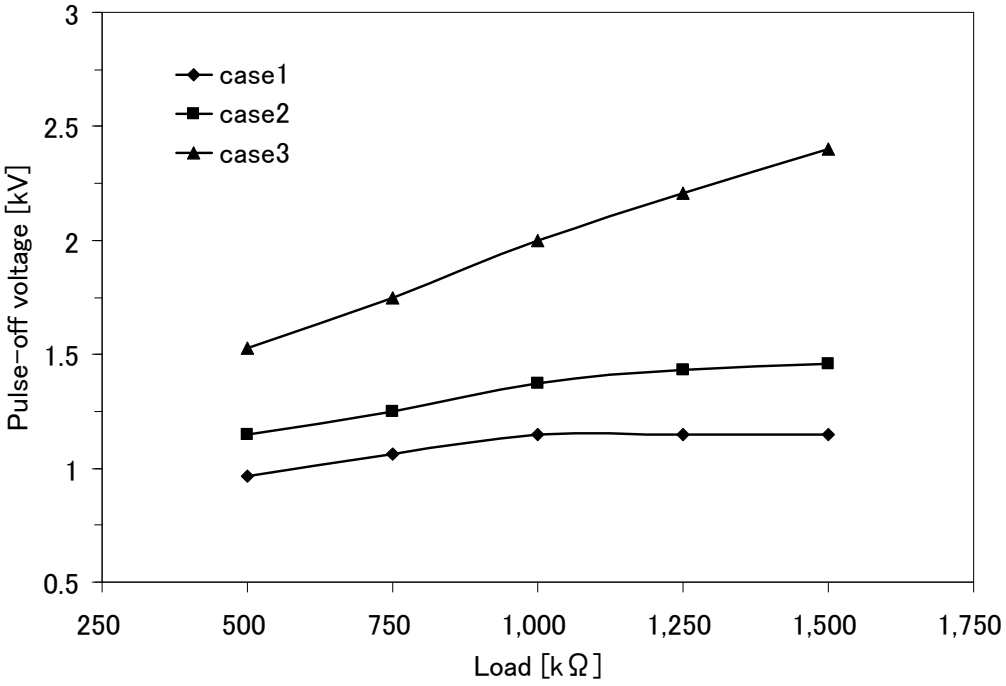

Figure 3.4: Measured pulse-off voltage versus R_{load} for cases 1, 2, and 3 shown in Figure 3.1

3.1.1.2 Effect on the rise/fall times and pulse width of the pulse voltage

Changes in the rise and fall times can be compared when the R_{load} is fixed. An example is shown in Table 3.1, which gives the rise and fall times for cases 1, 2, and 3 in Figure 3.1 when R_{load} is 1 MΩ, as well as the minimum pulse widths, calculated by simply adding the rise and fall times.

The pulse width is an important parameter because it determines the length of a nanofibre. Figure 3.5 illustrates the effect on the pulse width of varying the R_{load} for cases 1, 2 and 3. The scale shown represents the pulse width that was applied for non-continuous electrospinning for the purpose of this research: 80-400 ms. Increasing resistance resulted in a small or no change in the pulse widths for cases 1, 2 and 3; the pulse width is longest for case 3. The pulse widths for cases 1 and 2 are almost identical, showing only a slight difference. Controllability of the power and control module permits a desired output pulse width to be obtained independent of

the R_{load} by adjusting the width of the LM555 output to compensate for any differences caused by the load or circuit parameters.

Table 3.1: Rise/fall times and minimum pulse widths for cases 1, 2, and 3 in Figure 3.1 when R_{load} is 1 MΩ

Case	Rise time [μs]	Fall time [μs]	Minimum pulse width [μs]
1	3.27	164.00	167.27
2	3.30	164.00	167.30
3	3.34	210.00	213.34

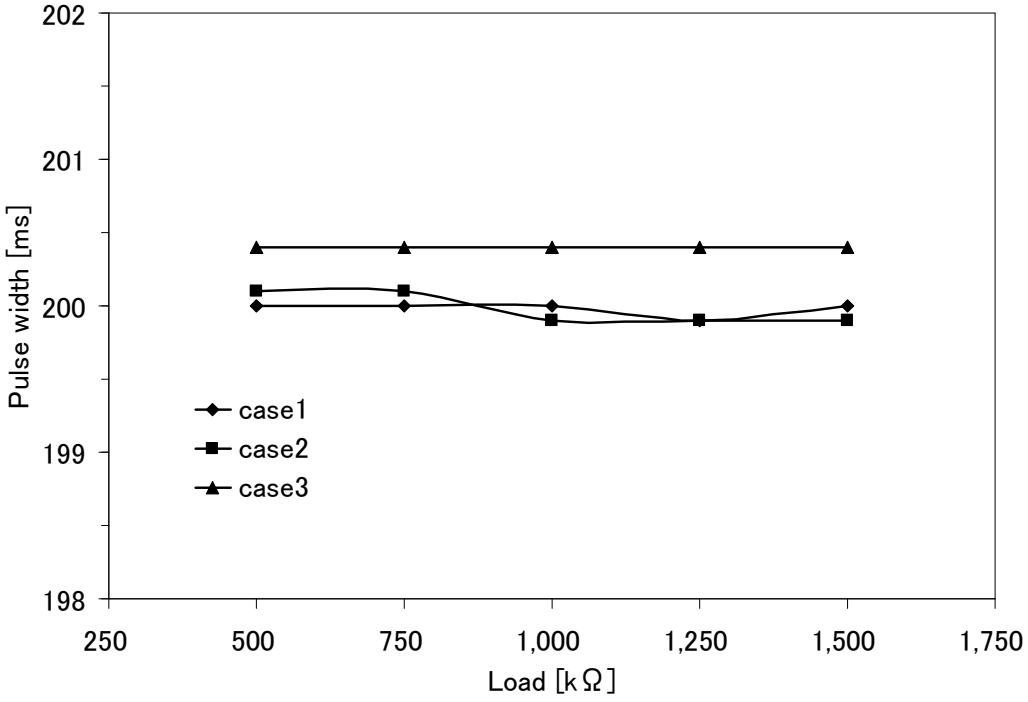

Figure 3.5: Measured output pulse width versus R_{load} for cases 1, 2, and 3 in Figure 3.1

3.1.2 Series-connected IGBTs

The series-connected IGBTs with the external circuits for voltage sharing were tested using varying resistive loads. Figure 3.6 shows the series-connected IGBTs with the external circuits for voltage sharing. Figure 3.7 shows samples of the output pulsed voltages produced when the R_{load} is 1 MΩ.

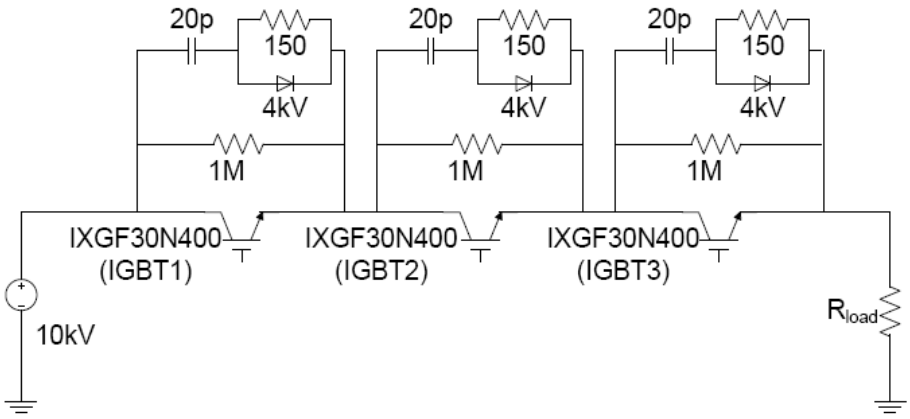

Figure 3.6: Series-connected IGBTs with the external circuits for voltage sharing

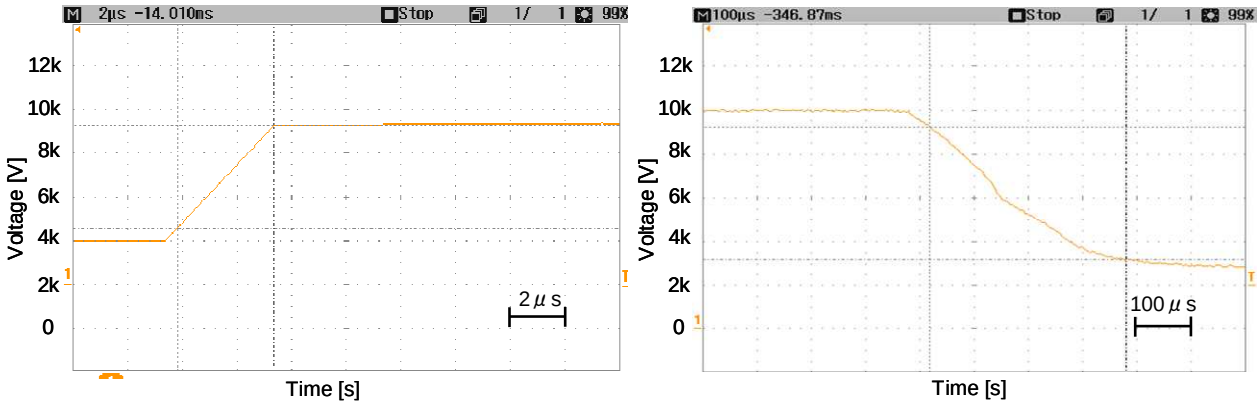

(a) (b)

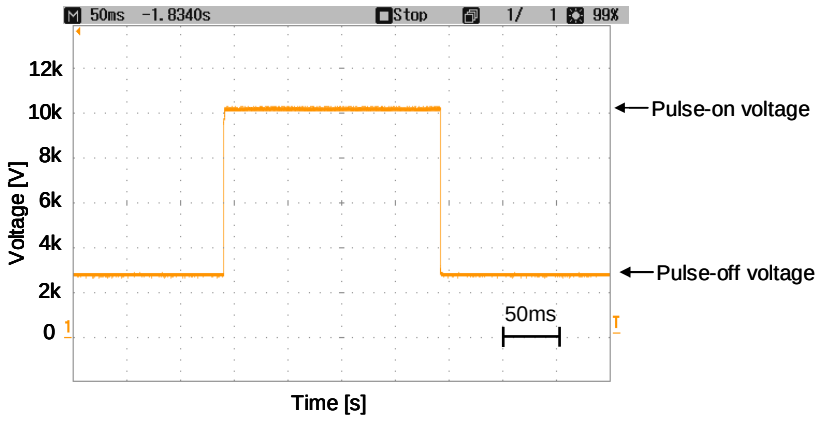

(c)

Figure 3.7: Measured output voltage waveform for series-connected IGBTs with the external circuits when the R_{load} is 1 MΩ: (a) pulse rise time (b) pulse fall time (c) a complete pulse waveform

3.1.2.1 Effect on the pulse-on and pulse-off voltages

Figures 3.8 and 3.9 illustrate the effects of varying the R_{load} on the pulse-on and pulse-off voltages, respectively. As Figure 3.8 indicates an increase in R_{load} results in a small or no change in the pulse-on voltage. On the other hand, as shown in Figure 3.9, an increase in load resistance results in a proportional increase in the pulse-off voltage, similar to that for case 3 in Figure 3.4. The pulse-off voltages increased by 155 % when the R_{load} varied from 750 kΩ to 1500 kΩ.

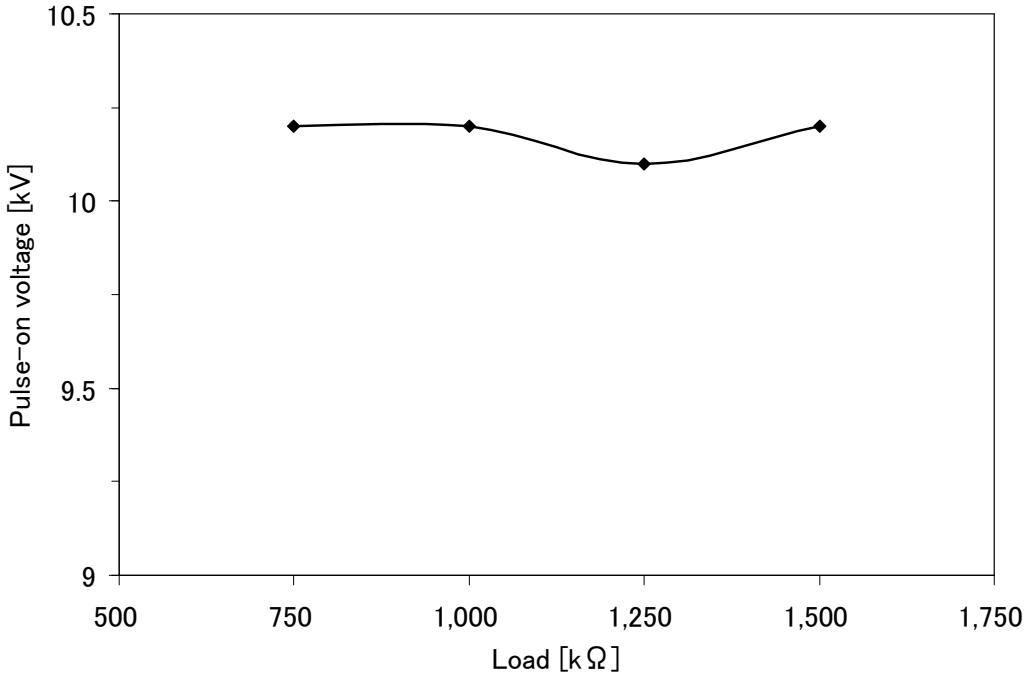

Figure 3.8: Pulse-on voltage versus R_{load} for series-connected IGBTs with the external circuits

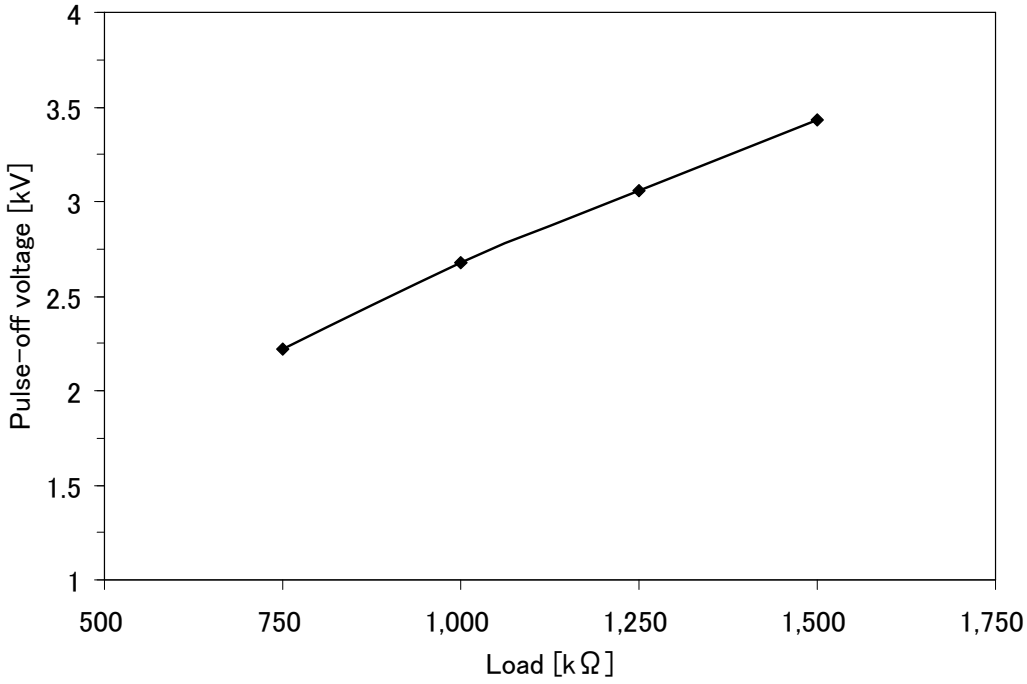

Figure 3.9: Pulse-off voltage versus R_{load} for series-connected IGBTs with the external circuits

3.1.2.2 Effect on the rise/fall times and pulse width of the pulse voltage

An example of the rise and fall times when the R_{load} is 1 MΩ is shown in Table 3.2, as well as the minimum pulse width, calculated by simply adding the rise and fall times. Figure 3.10 illustrates the effect of varying the R_{load} on the pulse width. A change in resistance does not influence the value of the pulse width.

Table 3.2: Rise/fall times and minimum pulse width for series-connected IGBTs when the R_{load} is 1 MΩ

Rise time [μs]	Fall time [μs]	Minimum pulse width [μs]
3.29	316.00	319.29

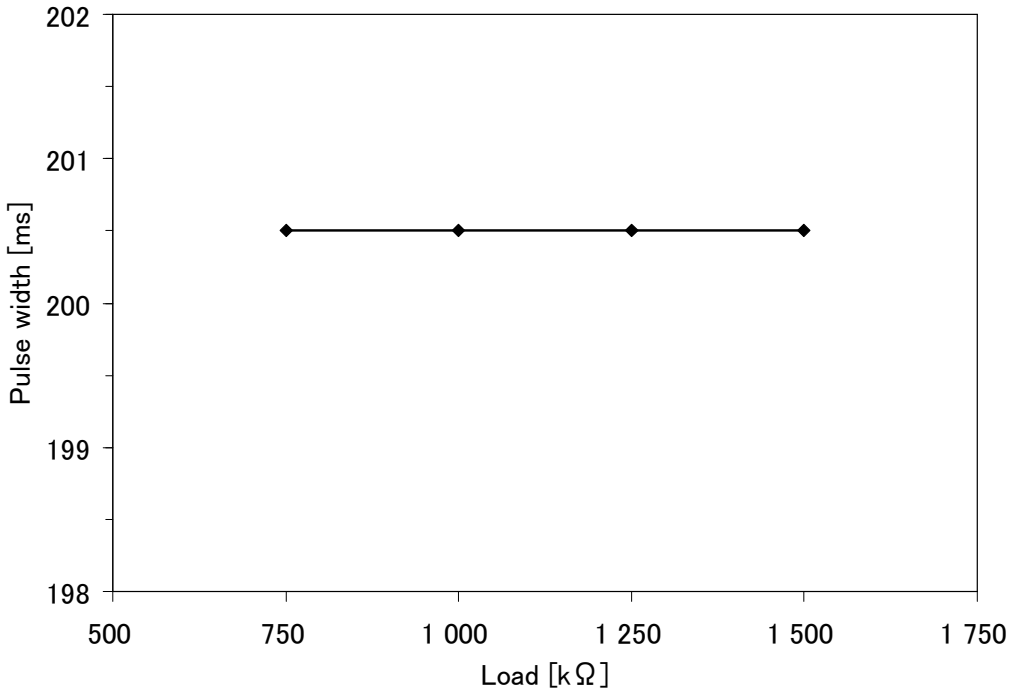

Figure 3.10: Measured output pulse width versus R_{load} for series-connected IGBTs with the external circuits for voltage sharing

3.1.2.3 Voltage distribution of the series-connected IGBTs

The external circuit for sharing voltage equally among the all IGBTs are used. To avoid damage, it is important that the voltage on the IXGF30N400 IGBT, not surpass 4 kV voltage rating. The output voltage measurements for each IGBT were taken with 10 kV applied and a load of 1 MΩ.

Figure 3.11 illustrates the measured voltage for IGBT 1 in Figure 3.6 when the IGBTs are open, as an example. Table 3.3 shows the measured voltages for all three IGBTs. The readings in Table 3.3 are when the IGBTs are off. The difference between the highest and the lowest maximum voltages is 0.18 kV. The maximum voltages for the three IGBTs are all within 4 kV, the voltage rating of the IXGF30N400. Even after the addition of overshoot voltages to each maximum voltage, all the IGBTs can be operated within 4 kV. The difference between the highest and lowest overshoot voltages is 0.05 kV, and that between the highest and lowest

undershoot voltages is 0.13 kV. The difference in the pulse widths of the three IGBTs is negligible.

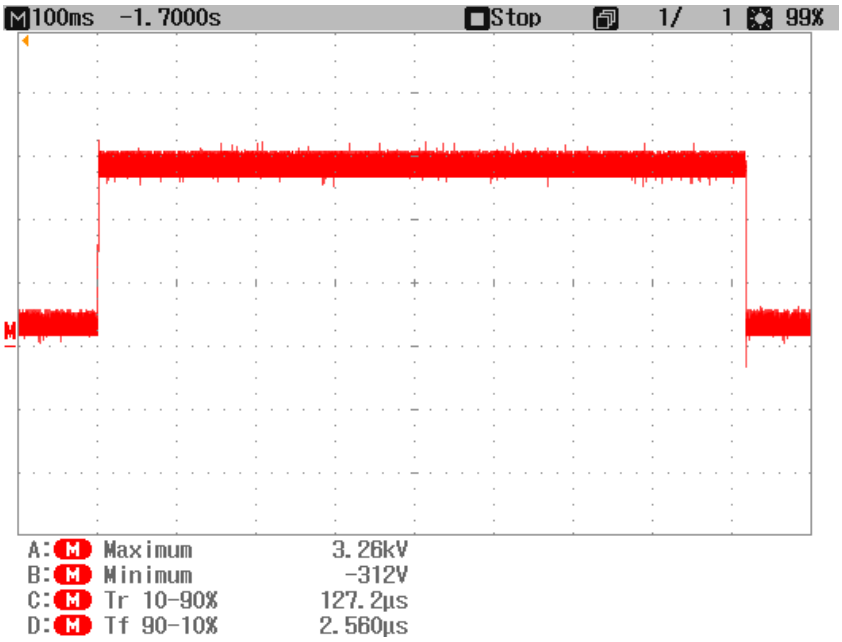

Figure 3.11: Measured voltage waveform across IGBT 1 when the IGBTs are open

Table 3.3: Measured voltages across the series-connected IGBTs

IGBT	Vmax [kV]	Vmin [kV]	Overshoot [kV]	Undershoot [kV]	Pulse width [ms]
1 : left	3.05	0.14	0.18	0.67	815.90
2 : middle	2.87	0.09	0.15	0.72	816.00
3 : right	2.90	0.12	0.20	0.80	815.90

3.1.3 The pulse-on and pulse-off voltages for non-continuous-mode electrospinning

A determination of the pulse-on and pulse-off voltages that are applied for non-continuous-mode electrospinning was necessary. To start a jet, the pulse-on voltage must be above the threshold voltage. The pulse-on voltage also influences the morphology of the nanofibres. To stop a jet, the pulse-off voltage must be below the threshold voltage. The threshold voltage must therefore be found so that the pulse-on and pulse-off voltages can be determined. To find

the threshold voltage, different magnitudes of DC voltage were applied to the electrospinning apparatus. The electrospinning apparatus used in this research is described in section in 2.2.2, but the pulse circuit was removed so that the DC voltages could be applied. A 150 mm gap distance between the needle and the collector was selected. The PEO 5 % solution used is described in section 2.2.1.1. By controlling the magnitude of the applied DC voltage to the electrospinning apparatus, different types of droplets and jets from the needle were observed corresponding to different levels of DC voltages, as shown in Figure 3.12. In order to explain an electrospinning process, droplets, and small droplets broken from the main droplet are defined in Figure 3.13.

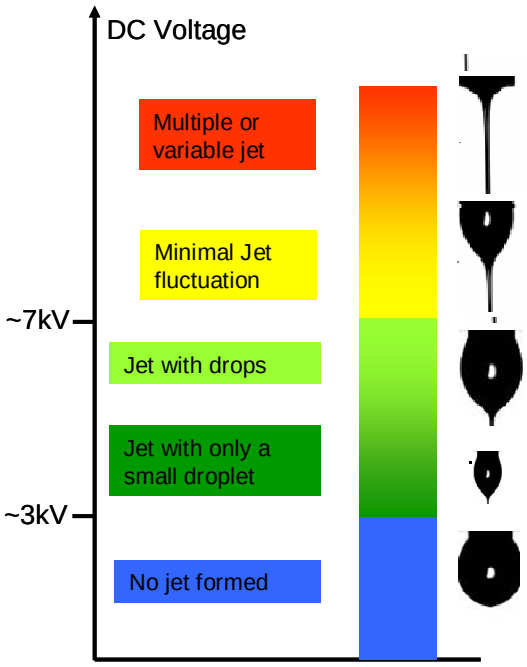

Figure 3.12: Types of droplets and jets as a function of applied DC voltage

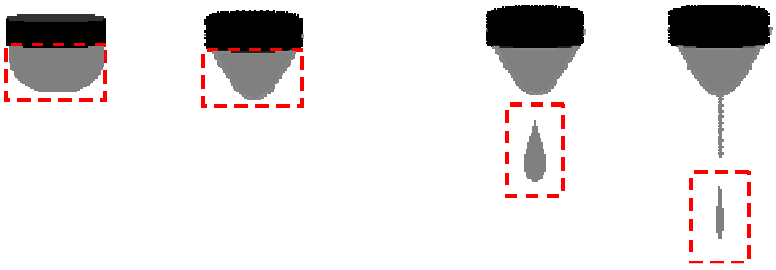

(a) (b)

Figure 3.13: Definitions of electrospinning process: (a) formation of a droplet (b) formation of a small droplet broken from the main droplet

As can be seen from Figure 3.12, no electrospinning was observed when the applied voltage was below 3 kV because the charges within the droplet are not high enough to overcome the surface tension to initiate the jet. In the range of 3-5 kV, the electrified jet is ejected from the droplet only when its volume is small. The charges within the droplet are higher than at voltage lower than 3 kV; however, they are not strong enough to consistently initiate a jet. As the volume of the droplet becomes larger, the jet could not be ejected, and the surface tension can no longer hold the large droplet, which then falls downward. It would thus destroy any nanofibres accumulated on the collector. The process was repeated. For the range of 5-7 kV, the electrified jet is always ejected; however, the droplet occasionally falls downward because the jet is not strong enough to consume the entire volume of the droplet. In the range of 7-15 kV, the Taylor cone seems stable, the electrified jet is always ejected, and no droplet drops onto the collector. At an applied voltage of 15 kV, the Taylor cone is no longer observed, the jet seems to emanate directly from the needle, and multiple jets are occasionally ejected. It is possible that the Taylor cone moves inside the needle. After considerations, it seems that the pulse-on voltage must be in the range of 7-15 kV for a stable jet to be ejected and that the pulse-off voltage must be below 3 kV in order to stop the jet when the gap distance between the needle tip and the collector is 150 mm.

The determination of the pulse-on voltage was based on consideration of the following factors. The experience gained in the research revealed that the diameter of nanofibres becomes thinner as the applied voltage is increased in the range of 7-15 kV if the gap distance between the needle and the collector is adjusted. As well, the pulse-on voltage is limited 12 kV due to the withstand voltage of the pulsed supply of the series-connected IGBTs. However, applying a voltage up to 10 kV to the three IGBTs is preferable for safety reasons. Even after adding the external circuits in order to share the total voltage, the voltage distribution to each IGBT is not perfectly equal as mentioned in section 3.1.2.3; hence, if 12 kV is applied to the three IGBTs, one IGBT might have more than the 4 kV rating voltage. Based on these considerations, a pulse-on voltage of 10 kV was chosen.

From Figure 3.9, it can be seen that the pulse-off voltage depends on the load resistance, which is, the wave shaping resistor described in section 2.1.4. The pulse-off voltage is below 3 kV when the load resistance is smaller than 1200 kΩ. Of course, as the load resistance decreases, the current of the pulse circuit increases, resulting in higher power demand from the

DC source and higher power consumption by the wave shaping resistor. These considerations led to the selection of approximately 2.7 kV as the pulse-off voltage, which makes the value of the wave shaping resistor 1 MΩ, which was obtained from the result of the experimental results indicated in Figure 3.9.

Figure 3.14 shows a sample of the output pulse voltage across the electrospinning apparatus in parallel with the 1 MΩ wave shaping resistor.

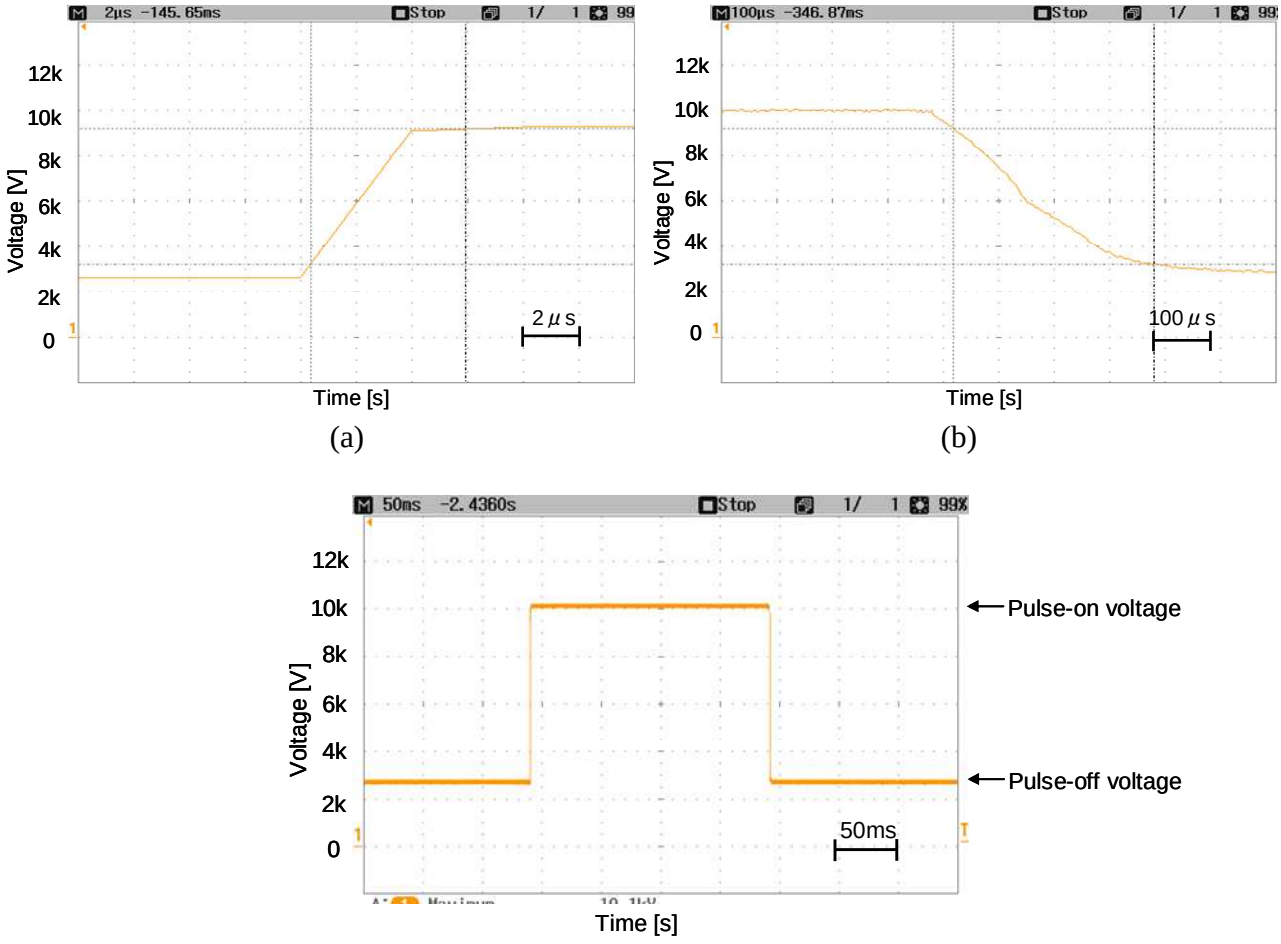

Figure 3.14: Measured output voltage waveform across the electrospinning apparatus in parallel with the 1 MΩ wave shaping resistor: (a) pulse rise time (b) pulse fall time (c) a complete pulse waveform

3.2 Results of non-continuous-mode electrospinning

This section provides an examination of the influence of the jet, the droplet, the diameter, and the bead formation of the fibres using a PEO solution and varying parameters such as the pulse width, the duty ratio of the pulse voltage, and the gap distance between the needle and the collector. For many biomedical applications, natural polymers such as alginate, provide a distinct advantage over synthetic materials. Non-continuous-mode electrospinning using blended solutions of varied volume ratios of alginate and PEO was therefore investigated.

3.2.1 Non-continuous-mode electrospinning with a PEO solution

The effects on the jet, the droplet, the diameter and the bead formation of the fibres of changing parameters such as the pulse width, the duty ratio of the pulse voltage, and the gap distance between the needle tip and the collector were investigated. A specific width of pulse-on voltage is required in order to start an electrified jet, and the width of the pulse-on voltage also influences the length of the nanofibres. A specific width of pulse-off voltage is also required to ensure that the jet can be stopped. In addition, the balance of the pulse widths of the turn-on and turn-off voltages is important because of the following factors. During the pulse-off voltage, the size of the droplet accumulated is affected by the gravity to the earth and the syringe pump. During the pulse-on voltage, an electrified jet is ejected from the droplet. The accumulated amount of polymer and the ejected amount of polymer should be the same. Otherwise, if the accumulated amount of the polymer is larger than the ejected amount, small droplets break up from the main droplet and fall on the collector. The disadvantages of falling droplets onto the collector are the waste of the polymer solution, and more importantly damage to the nanofibres already collected on the collector. The parameters of the periods and pulse widths that were applied to the electrospinning apparatus are shown in Table 3.4.

The influence of the gap distance between the needle tip and the collector was also examined. Changing the distance between the tip and the collector has a direct influence on both the flight time and the electric field strength. For the purposes of these researches, the pulse-on voltage of 10 kV and the pulse-off voltage of 2.7 kV were chosen to be applied for

Table 3.4: Pulse parameters of the pulse voltages

Case	Period [ms]	Pulse width [ms]	Duty ratio [%]
1	100	20	20
2	100	40	40
3	200	40	20
4	200	80	40
5	500	100	20
6	500	200	40
7	1000	200	20
8	1000	400	40

the electrospinning apparatus. To find an optimal gap distance, the distances between the needle tip and the collector were set at 100, 150 and 200 mm.

For all of the parameters of the pulse voltages applied to the electrospinning apparatus when a gap distance between the needle tip and the collector is 100 mm, the acceleration of the jet seems so strong that the straight jet hits the collector, and therefore no fibres are obtained. On the other hand, a gap distance of 150 mm is long enough that the jet is elongated and the solvent to evaporate before it hits the collector. It is collected as nanofibres. The electric field strength is strong enough to start a jet. With a gap distance of 200 mm, the electric field strength is not strong enough to start a jet. The optimal gap distance for this research was therefore determined to be 150 mm. The following results were obtained from experimental apparatus using a 150 mm gap.

Figure 3.15 shows the changes in the droplet and jet formations using case 6 from Table 3.4 as an example. The changes in the droplet and jet formations were recorded with a video camera. Then, the frames of the video as photo images were saved by the software, SC video cut and split manufactured by Softwareclub. Figure 3.15 (a) shows the droplet that was accumulated during the pulse-off voltage. The pulse-on voltage was applied to the needle where the droplets were to be prepared. When the voltage is applied, the meniscus of the liquid deforms into a Taylor cone, and a jet of the liquid is then ejected from the cone as shown in Figure 3.15 (b). The time for the Taylor cone to form and then for a jet to eject is denoted as T_{form}. To set a standard, the time for the event shown in Figure 3.15 (b) was determined to be $T = T_{form} = 0$ s. Figure (c) shows the jet before it became stable. As can be seen from Figures 3.15 (d) and (e), the stable jet was observed during T = 66-200 ms. At T = 200 ms in Figure 3.15 (f),

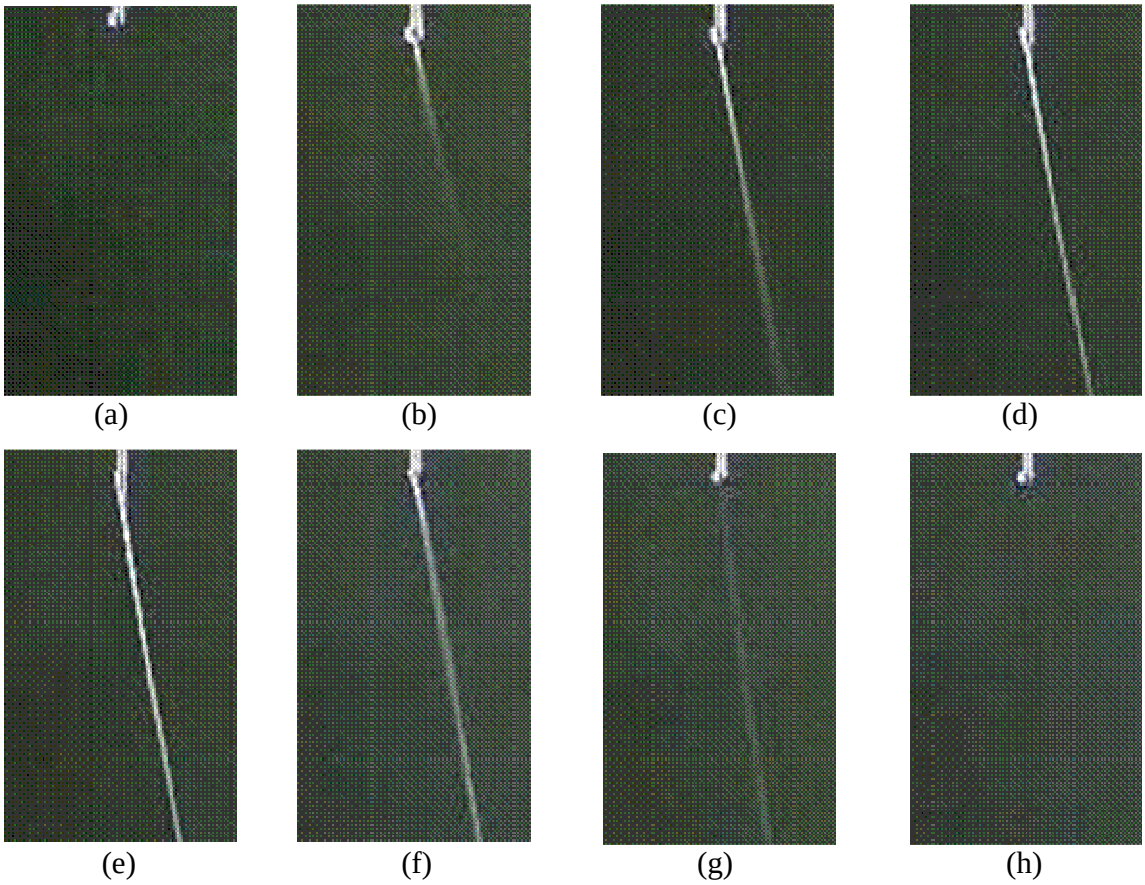

Figure 3.15: Droplet and jet formations produced by the pulse voltage, T=500 ms, D=40 %: (a) During the pulse-off voltage (b) T = T_{form} = 0 s (c) T = 33 ms (d) T = 66 ms (e) T = 100 ms (f) T = 200 ms: the pulse-off voltage has begun to be applied (g) T = 233 ms (h) T = 266 ms

the voltage was turned off. Sixty-six ms after the voltage was turned off, the jet completely disappeared, and the cone returned to the initial meniscus, as can be seen in Figure 3.15 (h).

For cases 1, 2, and 3 in Table 3.4, no jet was observed. In case 5 from Table 3.4, a jet is ejected during the turn-on voltage only when the droplet is small. As the droplet becomes larger, the charges from the turn-on voltage can not overcome the surface tension sufficiently for a jet to be initiated. As a result, the droplet accumulates by its gravity to the earth and the syringe pump, and falls downward. In cases 4, 6, 7, and 8, the jet is always ejected during the turn-on voltage; however, the droplet occasionally falls downward.

To collect samples of the fibres on the collector, aluminum foil was placed on the collector. A field emission scanning electron microscope (FE-SEM) was used to examine the diameter

and the morphology of the fibres, and the small droplets on the aluminum foil. Figure 3.16 shows a sample SEM image, in this instance, the results from case 7 in Table 3.4. The fibres, the beads inside the fibres, and the small droplets can be observed. Figure 3.17 shows the more magnified SEM images of the respective cases 4-8. It can be seen that the diameters of the most fibres in all cases are in the range of 100-400 nm.

A voltage of 10 kV DC was applied to the electrospinning apparatus in order to compare the morphology of the fibres obtained with a DC voltage with those from the pulse voltages. Gap distances of 150 and 200 mm were used between the needle tip and the collector. Figure 3.18 shows the SEM images of the samples produced by the DC voltage. Figure 3.18 (a) shows that the fibres are twisted rather than straight and that there were more droplets present than in Figure 3.17. The 150 mm distance is not long enough for the jet to evaporate its solvent before it hits the collector because the increased charges in the jet produced by the 10 kV DC compared to those in the jet produce by the 10 kV pulse voltages cause the jet to accelerate. As a result, there is insufficient time for the solvent to evaporate before it hits the collector. Figure 3.18 (b) shows that the fibres are straight, and that the diameters of most of the fibres are in the range of 50-200 nm. The 200 mm distance provides enough time for the solvent to evaporate before it hits the collector. Figure 3.18 (b) is therefore used as the basis of comparison with the fibres produced by the 10 kV pulse voltages.

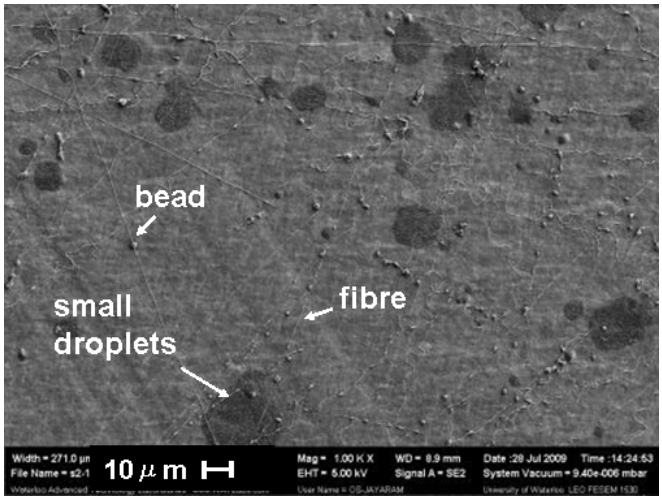

Figure 3.16: SEM image of the sample produced by the pulse voltage, T=1,000 ms, D=20 %

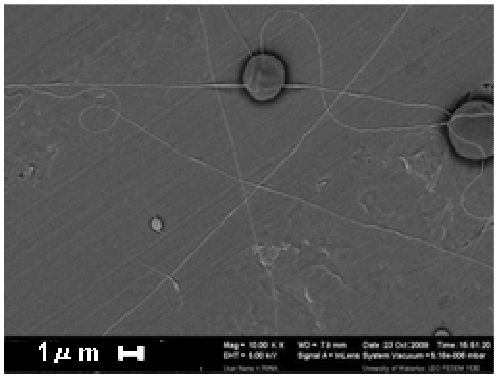

(a)

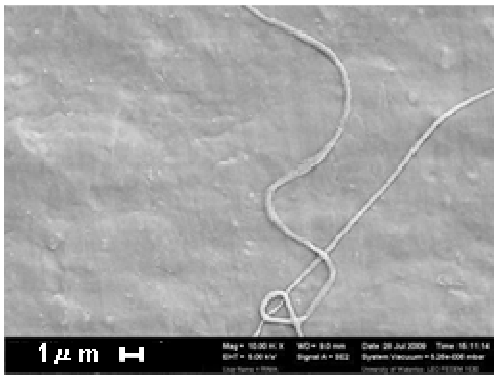

(b)

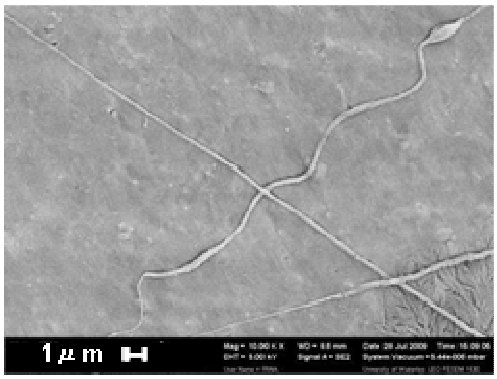

(c)

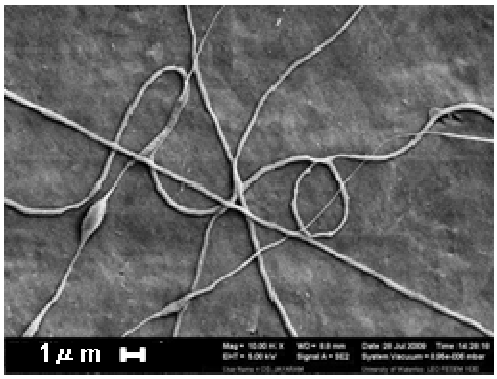

(d)

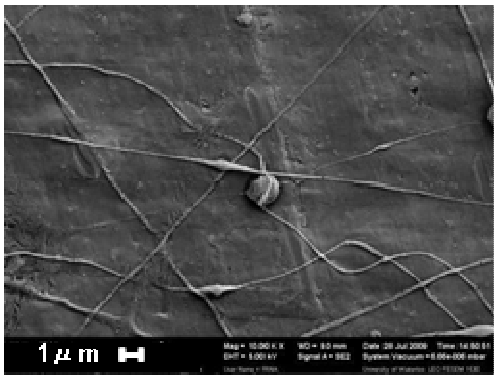

(e)

Figure 3.17: SEM images of the samples produced by the pulse voltages: (a) T=200 ms, D=40 % (b) T=500 ms, D=20 % (c) T=500 ms, D=40 % (d) T=1,000 ms, D=20 % (e) T=1,000 ms, D=40 %

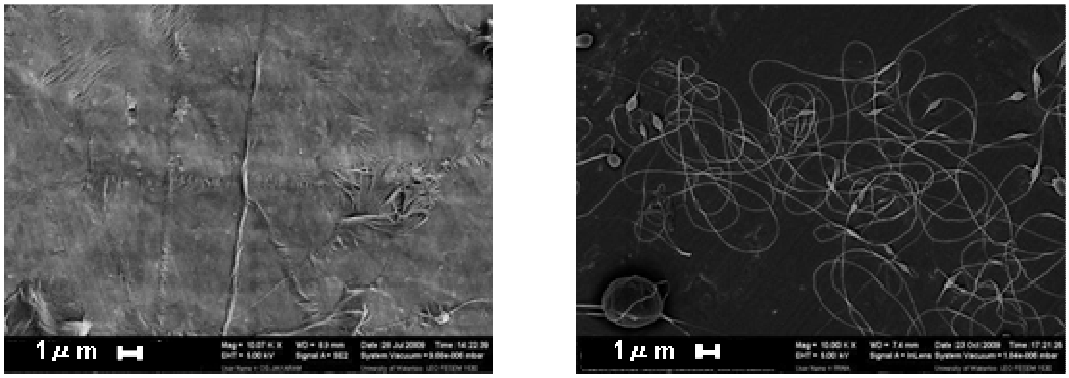

(a) (b)

Figure 3.18: SEM images of the samples produced by the DC voltage with varying distances: (a) 150 mm (b) 200 mm

3.2.2 Non-continuous-mode electrospinning with alginate/PEO blended solutions

The fabrication and chopping of the nanofibres with alginate and PEO blended solutions were investigated. As mentioned in section 2.2.1.2, electrospinning with only alginate is difficult, and the process has been successful only with polymers and polymer blends formed by blending alginate with PEO. For this reason, an alginate solution was blended with PEO. The 3 % alginate and the 3 % PEO used are the ones described in section 2.2.1.2. The following blend solutions created by varying the volume ratios of the alginate and the PEO were investigated: 20:80, 40:60, 60:40, and 80:20. A Con11/110 Conductivity/TDS handheld meter, manufactured by Oakton instruments, was used to measure the conductivities of the blended solutions, which are listed in Table 3.5. The gap distance between the needle tip and the collector was set at 150 mm. The pulse-on and pulse-off voltages applied were 10 kV and 2.7 kV, respectively. The period and the duty ratio of the pulse voltage were 500 ms and 40 %, respectively.

Table 3.5: Conductivities of the alginate/PEO blended solutions

Sample name	Volume ratio Alginate (3%) : PEO (3%)	Conductivity [ms/m]
A	20:80	83.2
B	40:60	156.6
C	60:40	398.0
D	80:20	612.0

As an example, Figure 3.19 shows the changes in the droplet and jet formation for sample B from Table 3.5. The changes in the droplet and jet formations were recorded with a video camera. Then, the frames of the video as photo images were saved by the software, SC video cut and split manufactured by Softwareclub. Figure 3.19 (a) shows the droplet that was accumulated during the pulse-off voltage. The pulse-on voltage was applied to the needle where the droplets were to be prepared. When the voltage is applied, a jet is ejected and then breaks up into small droplets as shown in Figure 3.19 (b). To set a standard, the time for the event shown in Figure 3.19 (b) was determined to be T = 0 s. Figure 3.19 (c) shows the straight jet before it became stable. As can be seen from Figures 3.19 (d) and (e), the stable jet was observed during T = 66-200 ms. At the T = 200 ms in Figure 3.19 (f), the voltage was turned off. Sixty-six ms after the voltage was turned off, the jet completely disappeared, and the cone returned to the initial meniscus, as can be seen in Figure 3.19 (h).

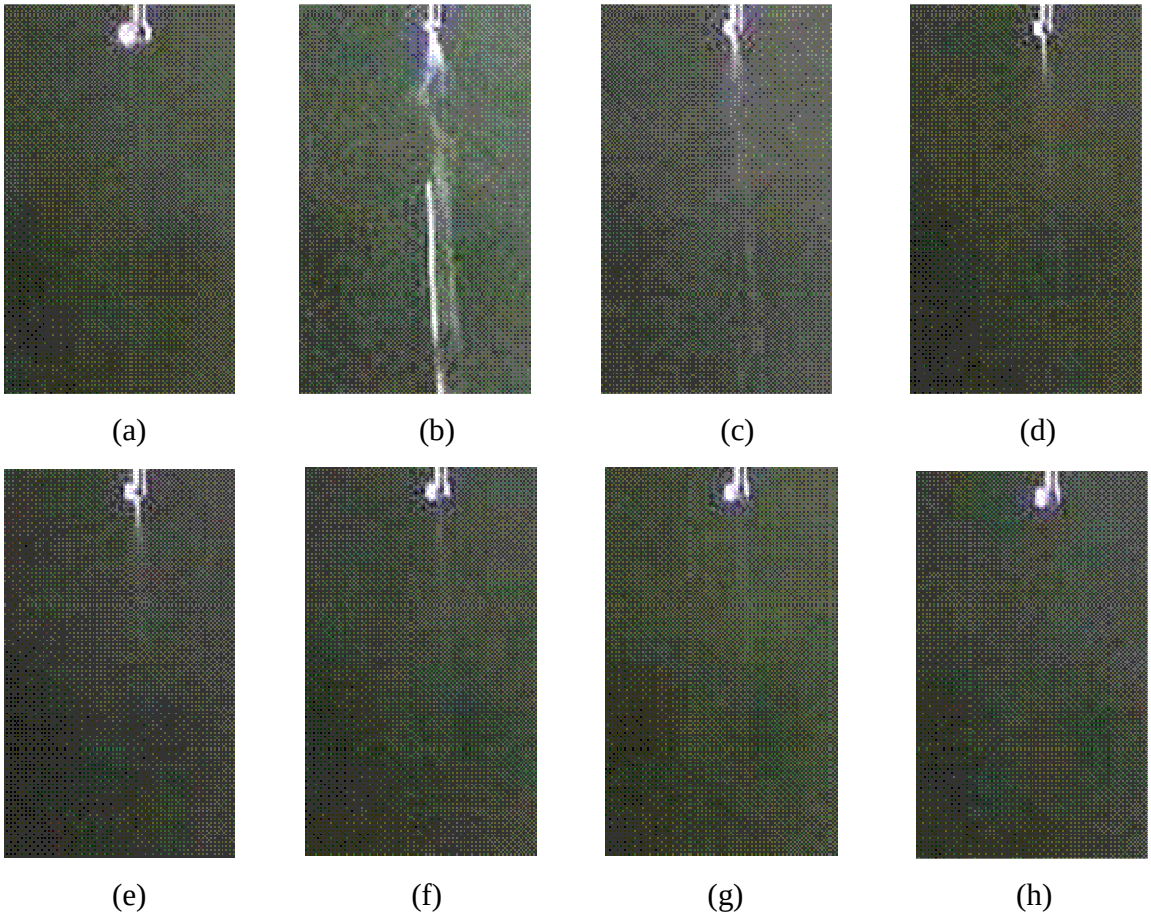

Figure 3.19: Droplet and jet formations of the alginate/PEO solution 40:60: (a) During the pulse-off voltage (b) T = 0 s (c) T = 33 ms (d) T = 66 ms (e) T = 100 ms (f) T = 200 ms: the pulse-off voltage has begun to be applied (g) T = 233 ms (h) T = 266 ms

In the cases when the volume ratios of the alginate and the PEO are 20:80, 40:60, and 60:40, the jet is always ejected during the turn-on voltage; however, the droplet occasionally falls downward. When the ratio is 80:20, no jet is observed.

As an example, Figure 3.20 shows the SEM image in the case of a volume ratio of 40:60. The fibres, the beads inside the fibres, and the small droplets can be observed. Figure 3.21 shows the more magnified SEM images for samples A, B, and C in Table 3.5. Figure 3.21 shows that the diameters of most of the fibres for all volume ratios are in the range of 30-40 nm.

A 10 kV DC voltage was applied to the electrospinning apparatus in order to compare the diameter and morphology of the fibres obtained by applying the DC voltage with those

produced by the pulse voltages. Figure 3.22 shows the SEM images of the sample produced by the DC voltage. As can be seen, the diameters of most of the fibres are in the range of 40-100 nm.

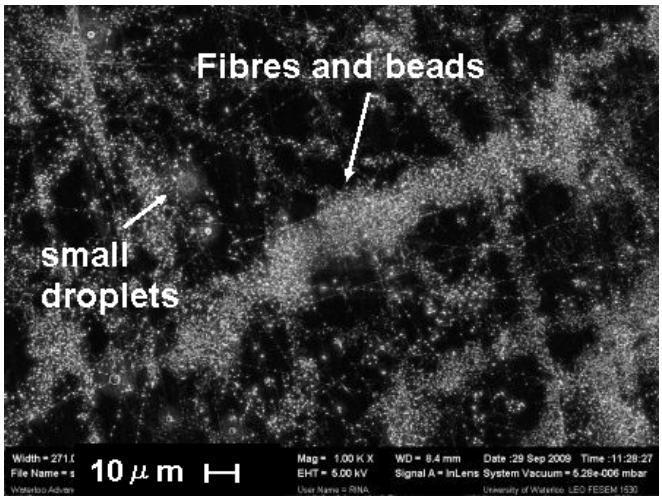

Figure 3.20: SEM image of the sample produced by the pulse voltage using the alginate/PEO solution 40:60

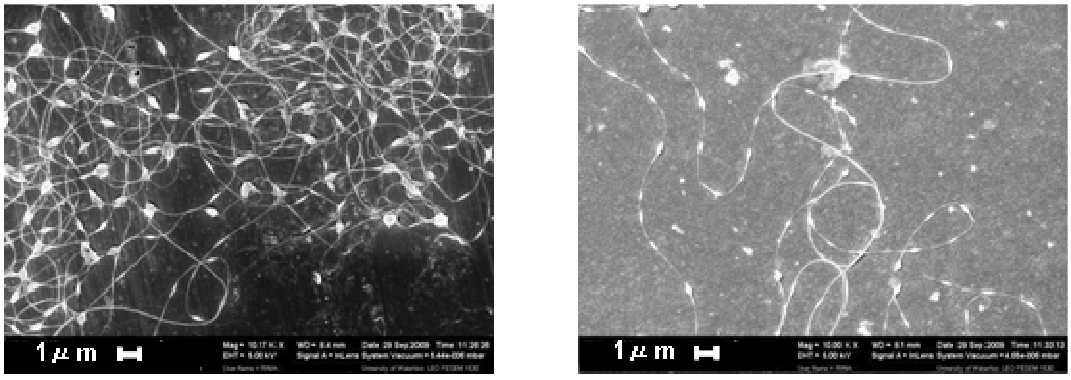

(a) (b)

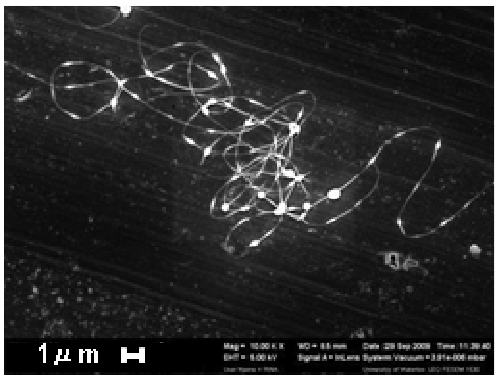

(c)

Figure 3.21: SEM images of the samples produced by the pulse voltage using the alginate/PEO solutions: (a) 20:80 (b) 40:60 (c) 60:40

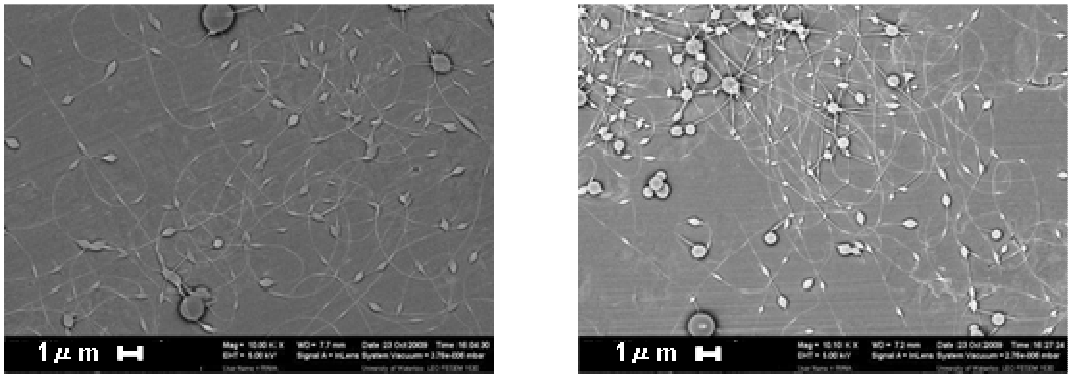

(a) (b)

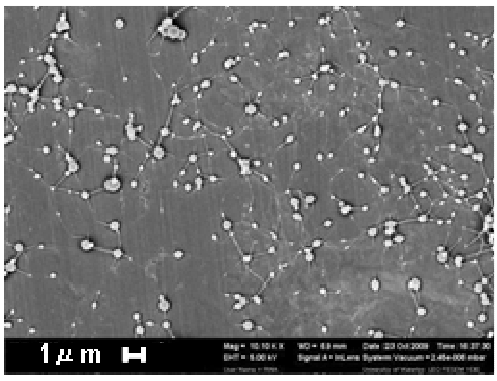

(c)

Figure 3.22: SEM images of the samples produced by the DC voltage using the alginate/PEO solutions: (a) 20:80 (b) 40:60 (c) 60:40

Chapter 4

Discussion

In this chapter, the results presented in Chapter 3 are used as a basis for discussion. The first experimental results considered are the effects on the output voltages of the single IGBT and the series-connected IGBT pulsed power supplies when the load resistance is varied. The results of the voltage distribution for each IGBT of the series-connected IGBT power supply are also examined. The next section discusses the results of the uses of the PEO solution and the alginate/PEO solution for non-continuous-mode electrospinning. These results are explained in detail and, whenever possible, are compared to similar results reported in the literature.

4.1 Performance of the pulsed power supply

4.1.1 Single IGBT

An ideal switch has a zero resistance during the on-state and infinite resistance during the off-state. In practice, transistors are not ideal switches. IGBTs have a small resistance in their conducting state and a high but not infinite resistance in their off state. Therefore, the pulse-on and pulse-off voltages vary when the load resistance is changed even if a high-voltage source output is fixed. According to Figure 3.3, an increase in load resistance results in a small or no change in the pulse-on voltage. On the other hand, an increase in load resistance results in an increase in the pulse-off voltage, as can be seen in Figure 3.4.

The change in pulse-on voltage is due to the change in the voltage drop across the on-state resistances of the IGBT switches. A small or no reduction was observed, as shown in Figure 3.3. The reason that an IGBT-based pulsed power supply experiences a small drop or no change is that IGBTs are minority carrier devices. In such devices, minority carriers are injected into the n^- drift region, resulting in a reduction in its resistance. The end result is that minority carrier devices have a small on-state resistance, unlike MOSFETs, which are majority carrier devices [55]. However, a drawback with these minority carriers is that they must be swept out in order for the device to turn off. Unfortunately, this procedure occurs through

recombination, which slows down the turn-off time, increasing the losses during turn-off and limiting the maximum switching frequency.

The change in pulse-off voltage is due to the change in the off-state resistance of the IGBT switches. Figure 4.1 shows the off-state resistances of the IGBTs when changing the load resistance in Figure 3.1. Based on the values from Figure 3.4, the off-state resistances can be calculated by using:

$$R_{off-state} = R_{load}\frac{V_{source} - V_{pulse-off}}{V_{pulse-off}} = R_{load} - \frac{4k - V_{pulse-off}}{V_{pulse-off}} \tag{4.1}$$

When the load resistance was changed from 500 kΩ to 1500 kΩ, the off-state resistance was increased by 237 % in case 1, 211 % in case 2, and 124 % in case 3 in Figure 4.1. The off-state resistance of a transistor is normally in the mega ohm range. It decreases with increasing temperature because the performance of semiconductors is dependent on temperature [56]. An increase in load resistance, resulting in a decreased current, then lowers the temperature of IGBTs. Therefore, increasing the load resistance causes an increase in the off-state resistance of IGBTs. This trend can be seen in cases 1 and 2 in Figure 4.1. The off-state resistance of case 2 is smaller than that of case 1 because the transient snubber in parallel with the IGBT in case 2 makes the total resistance smaller. The off-state resistance of case 3 stays at about 1 MΩ, as shown in Figure 4.1, due to the 1 MΩ resistance in parallel with the IGBT.

In general, a change in load resistance results in a change in the rise and fall times. A change in rise and fall times does not influence the pulse width that is applied for non-continuous-mode electrospinning, as can be seen in Figure 3.5. For the purpose of this research, the pulse width for non-continuous-mode electrospinning is 80-400 ms, which is large enough to render the change in rise and fall times negligible. Figure 3.5 shows that the longest pulse width occurs in case 3 because the rise and fall times of case 3 are also longer than those in cases 1 and 2, as shown in Table 3.1.

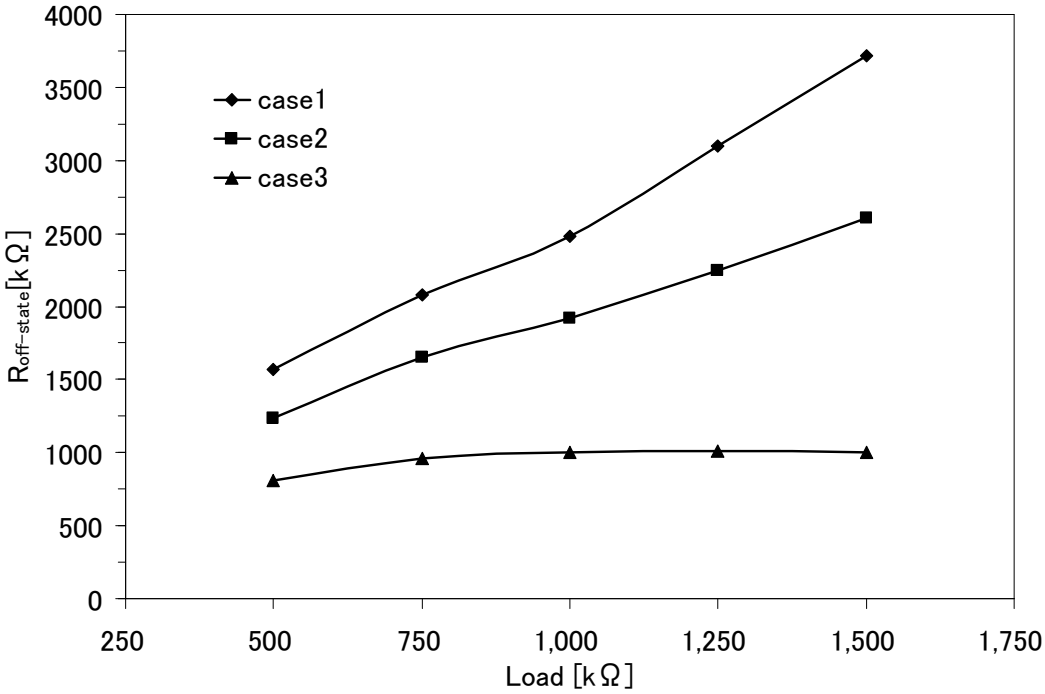

Figure 4.1: Off-state resistance of the IGBT versus R_{load} for cases 1, 2, and 3

4.1.2 Series-connected IGBTs

Based on the results shown in Figure 3.8, it can be stated that an increase in resistance results in a small or no change in the pulse-on voltage. On the other hand, according to Figure 3.9, an increase in resistance results in a proportional increase in the pulse-on voltage, a result similar to that for case 3 shown in Figure 3.4. The phenomena is the same as with one IGBT as discussed in section 4.1.1. The reason for a small or no change in the pulse-on voltage is that the IGBTs are minority carrier devices, which results in reduced on-state resistances. The change in pulse-off voltage is due to the change in the off-state resistance of the IGBT switches.

Substituting 10 kV for V_{source} and the pulse-off voltages from Figure 3.9 for $V_{pulse\text{-}off}$ in equation (4.1) gives the off-state resistances of the series-connected IGBTs when the load resistance is changed in Figure 3.6, as shown in Figure 4.2. As can be seen in Figure 4.2, increasing the load resistance causes an increase in the off-state resistance. The off-state

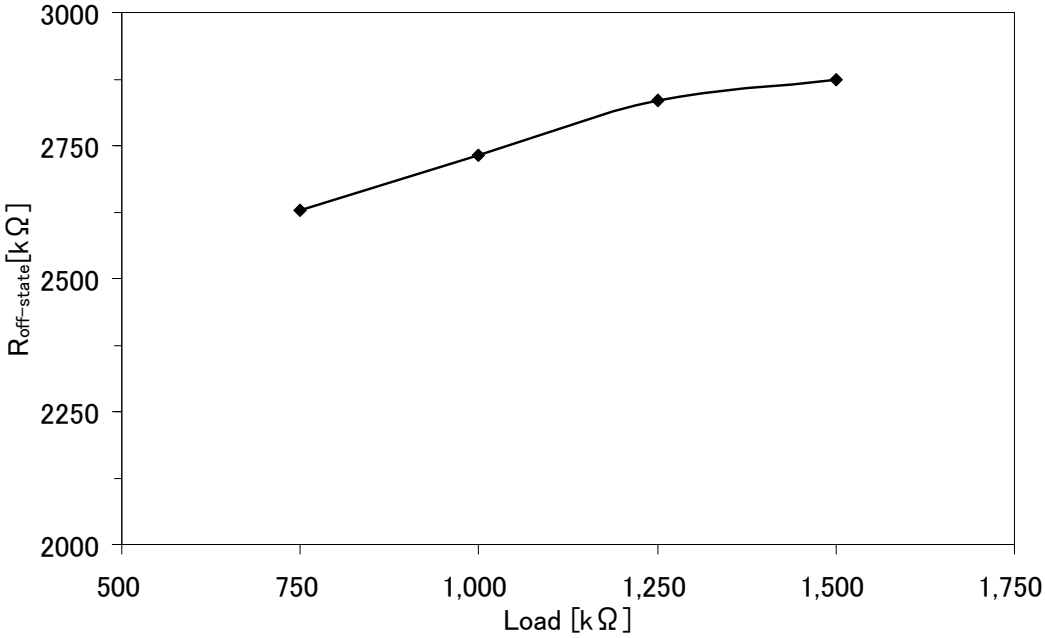

Figure 4.2: Off-state resistance of the series-connected IGBTs versus R_{load}

resistance increases by 109 % when the load resistance is changed from 750 kΩ to 1500 kΩ. The off-state resistance also decreases with increasing temperature. An increase in load resistance, resulting in a decreased current, lowers the temperature of the IGBTs. Therefore, increasing the load resistance causes an increase in the off-state resistance, as mentioned in section 4.1.1.

In general, a change in load resistance results in a change in the rise and fall times, which influences pulse widths when the pulse widths are very small. The pulse width for non-continuous electrospinning is large enough not to be influenced by a change in the rise and fall time, as can be seen in Figure 3.10.

The external circuits are used to share the voltages equally over several IGBTs in series connection. As can be seen in Table 3.3, although there is a 0.18 kV difference in the maximum voltages, the maximum voltages of all the IGBTs are within 4 kV. Even after the overshoot voltages are taken into consideration, all IGBTs can be operated within a safe range. The maximum voltage of IGBT 1 is relatively higher than that of IGBTs 2 and 3, the reason for which may be that the off-state resistance of IGBT 1 is higher than that of IGBTs 2 and 3 because the manufacturing process causes the characteristics of switches even with the same

part number to vary over a wide range. These variations can cause uneven voltage in the IGBTs even after adding the resistors for voltage sharing during steady-state; however, the voltage distribution of each IGBT is acceptable because it is within its safe operation range. Overshoot and undershoot voltages can be caused by imperfections in the existence of stray inductances of the wires. As can be seen in Table 3.3, there are 0.05 kV differences in the overshoot and undershoot voltage. The overshoot voltages are within the safety range since the total is under 4 kV after they are added to the maximum voltages as mentioned previously. After the value of the minimum voltage is considered, the lowest undershoot voltage is 0.08 kV. No description of the withstand voltage for the transient period is included on the datasheet of the IXGF30N400. However, 0.08 kV is assumed to be acceptable because the pulsed power supply was run for 10 hours without damaging the IGBTs. The difference in the pulse widths of the three IGBTs is 0.1 ms, which is considered negligible. The 0.1 ms difference is caused because switches, in general, do not naturally turn off at the same time, even if gating signals are applied simultaneously to all of them.

The pulse-on and pulse-off voltages were determined into 10 kV and 2.7 kV for non-continuous-mode electrospinning, respectively. Varying the pulse width and the duty ratio of the pulse voltage influences the jet, the droplet, and the diameter and the bead formation of the fibres. Next section discusses the experimental results of non-continuous-mode electrospinning using the series-connected IGBT pulsed power supply.

4.2 Non-continuous-mode electrospinning

4.2.1 Non-continuous-mode electrospinning with a PEO solution

This subsection discusses the experimental results of the non-continuous-mode electrospinning that are presented in section 3.2.1. To find the optimal gap distance between the needle tip and the collector, 100, 150, and 200 mm gap were examined because varying the distance has a direct influence on both flight time and electric field strength. In the case of the 100 mm gap distance, the jet has a short distance to travel before it reaches the collector plate. Moreover, the electric field strength increases at the same time, which also increases the

acceleration of the jet to the collector. As a result, there is not sufficient time for the solvents to evaporate before the jet hits the collector [1], and therefore no fibres are obtained. Increasing the gap distance to 150 mm, results in a decrease in the effect of the electrostatic field on the charged jet. The flight speed of the jet decreases with the increased distance and the time for the jet to fly from the needle tip to the collector is longer. The increase in the distance therefore results in the advantage of allowing the charged solution jet to split and elongate [23]. In the case of 200 mm gap, electrostatic field is not strong enough to overcome the surface tension; thus, a jet can not be initiated. Thus 150 mm gap was found to be the optimal distance.

The changes in the droplet formations and jets shown in Figure 3.15 are similar to those with the non-continuous-mode electrospraying mentioned in section 1.3.1. After the turn-on voltage is applied to the needle tip, the time T_{form} is the time required for a Taylor cone to form, and then a jet of the liquid is ejected from the cone, which requires less than 33 ms. Precise values of T_{form} can not be measured because of the 30 frames per second limitation of the software used, SC video cut and split. During T = 0-66 ms, the jet continues to eject but seems unstable, so it is called $T_{unstable}$. During T = 66-200 ms, the jet seems stable and is called T_{stable}. After the turn-on voltage is turned off, it takes approximately 66 ms for the jet to disappear, $T_{disapper}$. Due to the instability of the jet during T = 0-66 ms and 200-266 ms, the diameter of the nanofibre might be effected.

It is important to find the optimal period and duty ratio of the pulse voltage in order not to fall small droplets on the collector. In cases 1, 2, and 3 from Table 3.4, no jet was observed because the charges within the droplet are not high enough to overcome the surface tension so that the jet can be initiated. However, the electrostatic repulsion and the Coulomb force during the pulse-on voltage in addition to its gravity to the earth and the syringe pump cause the droplet to fall downward. In case 5, the jet is ejected during the turn-on voltage only when the droplet is small. This result means that the surface tension is too strong for jets to be initiated due to the large droplets accumulate during the pulse-off voltages. As a result, the droplet increasingly accumulates, and then falls on the collector without going through the electrospinning process. In cases 4, 6, 7, and 8, the jet is always ejected during the turn-on voltage, which means that the charges of the droplets can always overcome the surface tension of the accumulated droplets. An analysis of these results leads to the conclusion that the minimum pulse width that can initiate an electrified jet is approximately 80 ms for the

parameters used in this study. The following discussion is therefore based on the pulse width being longer than 80 ms. In the case of a 20 % duty ratio, there is always a jet during a pulse-on voltage for the pulse width of 1000 ms but not for one of 500 ms. The probability therefore exists that a longer period produces a more constant jet during the pulse-on voltage when the duty ratio is the same value. The data shows that it is highly likely that a jet is always ejected when the duty ratio of the pulse voltage is more than 40 % for the parameters used in this study. This finding means that a higher duty ratio tends to contribute a constant ejection during the pulse-on voltage, which is closer to 10 kV DC voltage having a constant jet, as mentioned in section 3.1.3.

The small droplets and beads inside the fibres were observed in all cases, and an example is shown in Figure 3.17. Figure 3.17 shows that the diameters of most of the fibres in all cases are in the range of 100-400 nm. The effect on the small droplet was mentioned in the previous paragraph. The morphology of the fibres, such as diameter and bead formation, is influenced by the polymer solution parameters, the processing conditions, and the ambient conditions, as mentioned in section 1.2.2. Of these parameters, the viscosity, the surface tension, the conductivity, the applied voltage, and the feed rate are especially important. In addition, the instability of the jet affects the bead formation of the fibres.

The beads and non-uniformity of the fibres are related to the instability of the jet solution [57, 58]. As previously explained, the jets seem unstable during T = 0-66 and 200-266 ms, as shown in Figure 3.15. The existence of the drops caused by unbalanced droplets that are accumulated and ejected, also lead to instability in the jet. A similar phenomenon was presented in [58], in which the feed rate led to the instability of the jet solution. When the feed rate exceeds a critical value, the delivery rate of the solution jet to the capillary tip exceeds the rate at which the solution is removed from the tip by the electric forces. This shift in the mass-balance results in the formation of a sustained but unstable jet and fibres with large beads. Even the jet during T = 66-200 ms showed instabilities, and [57] reported that the dominant of axisymmetric instability forms beaded fibres. The experimental results shows that higher voltages tend to suppress the formation of beaded fibres [57] because a higher voltage suppresses the axisymmetric instability [59, 60, 61]. As mentioned in section 3.1.3, however, the Taylor cone is no longer observed and multiple or unstable jets are ejected if the applied voltage exceeds 15 kV. There is therefore a good possibility that increasing the applied voltage

to values higher than 10 kV gives rise to higher electrostatic repulsion forces between the needle tip and the collector which in turn provides higher drawing stress in the jet, hence producing a smaller bead size, but the value should be lower than 15 kV in this study. As can be seen in Figure 3.18 (b), the diameters of most of the fibres produced by the DC 10 kV are in the range of 50-200nm, which are thinner than the 100-400 nm produced by the pulsed 10 kV because more charges built up by the electrospinning jet result in the stretching of the solution.

The viscosity of the solution influences the diameter and the bead formation of the fibres. A minimum level of viscosity is required in order to yield fibres without beads. As the viscosity of the solution is increased, the beads become larger, the average distance between beads longer, and the fibre diameter larger, and the shape of the beads changes from spherical to spindle-like [12, 13], as shown in Figure 3.17. Reference [13] showed that uniform fibres without beads can be obtained using a 3.8-4.3 % concentration of PEO with a weight of 900,000 in distilled water. Reference [62] showed that the fibres with diameters in the range of 100-275 nm without beads can be obtained using a 4 % concentration of PEO with a weight of 900,000 in distilled water. Using a 5 % concentration of PEO with a weight of 600,000, the fibres that were obtained in this research have diameters in the range of 100-400 nm produced by the pulse voltages, and 50-200 nm, as produced by the DC voltage with beads.

Reference [13] showed that varying the viscosity of the PEO solution in distilled water produces little change in the value of the surface tension. The surface tension is one of the factors that influences the diameter of the fibres and the bead formation. The surface tension coefficient depends on the polymer and the solvent. For example, changing the ratio of ethanol to water can change the surface tension coefficient of the PEO solution. Varying the concentration of the PEO solution from 1-4.5 % has little effect on the values of the surface tension but viscosity [13]. Surface tension is therefore not discussed further in this work since the only solvent used was distilled water.

Conductivity also affects the diameter of the fibres and the bead formation. Electrospinning involves the stretching of the solution, which is caused by the repulsion of the charges on its surface. Therefore, if the conductivity of the solution is increased, more charges can be carried by the electrospinning jet, thus resulting in the stretching of the solution. Further discussion of the conductivity of the solution is presented in section 4.2.2.

4.2.2 Non-continuous-mode electrospinning with alginate/PEO blended solutions

This subsection discusses the results of the testing of the non-continuous-mode electrospinning that are presented in section 3.2.2.

The changes in the droplet formations and the jets using the alginate/PEO 40:60 solution, are shown in Figure 3.19 and are similar to those with the PEO provided in Figure 3.15. The applied voltage causes the droplet to fall downward before the jet is initiated, as shown in Figure 3. 19 (b). This effect might occur because the surface tension of the droplet is too strong to initiate a jet. In fact, the size of the droplet shown in Figure 3.19 (a) is larger than that shown in Figure 3. 15 (a). The downward forces such as electrostatic repulsion, the Coulomb force, the gravity to the earth, and the syringe pump lead to the droplet falls downward without going trough electrospinning. During T = 0-66 ms, the jet is ejected, but seems unstable. During T = 66-200 ms, the jet seems stable. After the turn-off voltage is applied, it takes approximately 66 ms for the jet to disappear. When Figure 3.19 is compared with Figure 3.15, the width of the jet is larger and the droplet from the needle is smaller in Figure 3.19. The thinner electrified jet of polymer results in a larger droplet at the needle tip.

As can be seen from Table 3.5, a higher proportion of alginate creates a higher conductivity in the solution because sodium alginate is a polyelectrolyte, which has a high conductivity. In the case of an 80:20 volume ratio of the alginate to the PEO, no jet is observed. The strong repulsive force among the polycations could be the key factor that hinders electrospinning [54]. In the cases of 20:80, 40:60, and 60:40 volume ratios, the jet is always ejected during the turn-on voltage; however, the droplet occasionally falls downward. Blending the alginate with a specific volume of PEO can reduce the repelling force among the polycationic alginate molecules to a specific level, thus facilitating electrospinning [63]. The formation of nanofibres can also be enhanced because of hydrogen bonds between a polyelectrolyte and a non-ionogenic polymer such as PEO [64].

The drops and the beads inside the fibres were observed in the cases of 20:80, 40:60, and 60:40 alginate/PEO solutions and an example is shown in Figure 3.20. Figure 3.21 shows that the diameters of most of the fibres are in the range of 30-40 nm. The cause of the droplet and the influence on the morphology of the fibres by the instability of the jet, the viscosity and the

surface tension of the solution, the applied voltage, and the feed rate are discussed in section 4.2.1. Therefore, these are not examined further in this subsection.

The diameters in Figure 3.21 are at 30-40 nm, thinner than those with PEO, at 100-400 nm, because the conductivities of the alginate/PEO solutions are higher than that of the PEO solution, 7.6 mS/m. Electrospinning involves the stretching of the solution, which is caused by the repulsion of the charges on its surface. Therefore, if the conductivity of the solution is increased, more charges can be carried by the electrospinning jet, thus resulting in the stretching of the solution. The increase in the stretching of the solution tends to yield fibres with smaller diameters. The beads also become smaller and more spindle-like. As can be seen in Figure 3.22, the diameters of most of the fibres produced by the DC 10 kV are in the range of 40-100 nm, which is thicker than those produced by the pulsed 10 kV, 30-40 nm. The length of the straight jet portion provides an explanation of the thicker diameter of the fibres produced by the DC 10 kV. As shown in Figure 4.3, electrospinning processes consist of two modes: the straight jet portion and the whipping zone. Reference [65] showed that straight jet portion becomes longer as the electric field increases. If the distance between the needle and the collector is fixed, the length of the whipping zone therefore decreases as the electricfield increases, resulting in insufficient length for the solvent to evaporate before it reaches the collector. The result is fibres with thicker diameters and beads. The beads shown in Figure 3.22 are rounder than those shown in Figure 3.21, which are spindle-like. These results means that the whipping zone was not long enough for the jet to stretch. As mentioned in section 4.2.1, increasing the applied voltage produces a smaller bead size and a thinner diameter of the fibre; however, it is important that the distance between the needle and the collector be adjusted so that the applied voltage can be increased to obtain a smaller bead and a fibre with a thinner diameter.

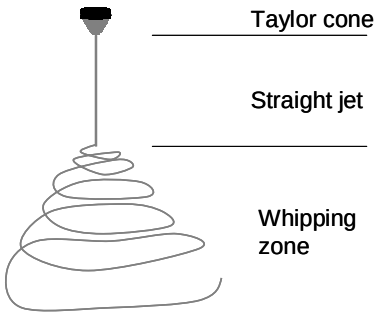

Figure 4.3: Straight jet portion and whipping zone of electrospinning process

Chapter 5
Conclusions and future research

5.1 Summary and conclusions

In this research, an IGBT-based pulsed power supply was designed and built for use in non-continuous-mode electrospinning. Electrospinning process requires a high voltage, but not a high current. The semiconductors with a high voltage rating and a high current rating are available in the market, but the semiconductor that is suitable for the pulsed power supply for this research is not available. Therefore, the semiconductors which have high voltage ratings and medium current ratings, IXGF30N400 IGBTs, were connected in series. The external circuits were used to equalize the voltage among the series-connected IGBTs during steady-state as well as turn-on and turn-off transients. A wave shaping resistor was connected in order to reduce the resistance at the load so that the required pulse-off voltage could be obtained. Since precise control of the pulse parameters is required for the application of pulsed high voltages, especially when it is necessary to optimize a process, a timer LM555 was used. The LM555 provides a control of the pulse width and the duty ratio. This pulsed power supply is capable of producing controllable square pulses with amplitudes up to 10 kV and widths of a few hundred micro seconds to DC.

The effects of varying the load resistance from 500 kΩ to 1500 kΩ and from 750 kΩ to 1500 kΩ on the output pulse of the single IGBT and of the series-connected IGBT pulsed power supplies were studied. An increase in resistance results in a small or no change in the pulse-on voltages of the IGBT-pulsed power supplies because IGBTs are minority carrier devices. In contrast, an increase in resistance resulted in an increase in the pulse-off voltages. The change in the pulse-off voltages is due to the change in the off-state resistance of the IGBTs. Increasing the load resistance causes increases the off-state resistance of the IGBTs. The off-state resistance of the single IGBT is increased by 237 % in case 1, 211 % in case 2, 124 % in case 3, as shown in Figure 4.1, and that of the series-connected IGBTs is increased by 109 % as shown in Figure 4.2, when load resistance is changed from 500 kΩ to 1500 kΩ and from 750 kΩ to 1500 kΩ, respectively. The external circuits were used to share the voltage equally over IGBTs in series. The voltage distribution of each IGBT was not perfectly equal

even after the external circuit for voltage sharing were connected to the IGBTs; however, the distribution is acceptable due to its safe operating range.

In conclusion, the pulse parameter of the output voltage can be controlled by the circuit parameters such as the number of series IGBTs, the load resistance, and the parameters of the gating pulses generated by the LM555.

The series-connected IGBT pulsed power supply was used to fabricate and chop nanofibres. Two polymers were chosen for the preparation of the solutions: PEO and alginate. Nanofibres were successfully fabricated and chopped with the PEO solution using the pulsed power supply. It is important to determine the optimal period and duty ratio of the pulse voltage so that droplets do not destroy the nanofibres that are already collected onto the collector. An examination of eight cases of pulse parameters leads to the minimum pulse width that can initiate an electrified jet is approximately 80 ms for the parameters used in this study. The probability therefore exists that a longer period produces a more constant jet during the pulse-on voltage when the duty ratio is the same value. It is also highly likely that a jet is always ejected during the pulse-on voltage when the duty ratio is 40 % for the parameters used in this study. This finding means that a higher duty ratio tends to contribute to constant ejection during the pulse-on voltage. The diameters of most of the fibres fabricated by the pulse voltages are in the range of 100-400 nm. The beads inside the fibres and the droplets on the collector were also observed. The diameters of most of the fibres produced by the DC 10 kV are in the range of 50-200 nm, which are thinner than those produced by the pulsed 10 kV because more charges built up in the jet result in the stretching of the solution. The main reason for the existence of the droplets is the unbalance of the periods between the pulse-on and pulse-off voltages. The bead formation and the non-uniformity of the fibres are caused mainly by the instability of the jet. The bead formation and the non-uniformity of the fibres are also influenced by the viscosity, the surface tension, the conductivity, the applied voltage, and the feed rate.

Blended solutions of the following varied the volume ratios of alginate and PEO were investigated: 20:80, 40:60, 60:40, and 80:20. In the case of the 80:20 volume ratio of alginate to PEO, no jet is observed. In the cases of volume ratios of 20:80, 40:60, and 60:40, the jet is always ejected during the turn-on voltage; however, the droplet occasionally falls downward. The diameters of most of the fibres are in the range of 30-40 nm. The diameters of the

alginate/PEO blended solution are thinner than those of the PEO solution because the conductivities of the alginate/PEO solutions are higher than those of the PEO solution. If the conductivity of the solution is increased, more charges can be carried by the jet, thus resulting in the stretching of the solution. The increase in the stretching of the solution tends to yield fibres with smaller diameters. However, the diameters of most of the fibres produced by the DC 10 kV are in the range of 40-100nm, which are thicker than those produced by the pulsed 10 kV. A longer straight jet portion due to more charges in the jet leads to shorter whipping zone. As result, the diameter of the fibres became thicker and the shape of the beads became rounder.

5.2 Future research

The 4 kV rating of the IGBT prompted the use of a pulsed power supply from three IGBTs in series, which enabled pulses of 10 kV to be produced. Future work could focus on increasing the number of IGBTs connected in series using the same method or the use of the switches with higher voltage ratings, in order to further increase the amplitude of the output pulse voltages. However, using more switches leads to a greater chance of poor synchronization of their commutation, which might result in damage to the switches. Switches that have higher voltage ratings with high-current ratings are available but are more expensive and not meant for this application due to their huge power rating.

The beads inside the fibres and the non-uniform diameters of the fibres are related to the instability of the jet solution. Some reports show that higher voltages tend to suppress these instabilities [59, 60, 61]. There is therefore a good possibility that increasing the applied voltage higher than 10 kV gives smaller bead size and more uniform fibre diameters. In addition, it is important to adjust the distance between the needle and the collector as the applied voltage is increased.

A higher applied voltage might also contribute to shorter time for a jet to be initiated and less time for a jet to be stable, leading to the determination of a better optimal period and the duty ratio of the pulse voltage so that the number of drops on the collector might be reduced.

References

[1] S. Ramakrishna, K. Fujihara, W.E. Teo, T.C. Lim, Z. Ma, *An Introduction to Electrospinning and Nanofibers*, Singapore: World Scientific Publishing Co. Pte. Ltd., 2005.

[2] C. Kriegel, A. Arrechi, K. Kit, D. J. McClements, J. Weiss, "Fabrication, Functionalization, and Application of Electrospun Biopolymer Nanofibers", *Critical Reviews in Food Science and Nutrition*, vol. 48, no. 8, pp. 775-797, Sept. 2008.

[3] J. S. Kim, D. H. Reneker, "Mechanical properties of composites using ultrafine electrospun fibers", *Polymer Composite*, vol. 20, no. 1, pp. 124-131, Feb. 1999.

[4] D. Li, Y. Xia, "Electrospinning of nanofibers: Reinventing the wheel?", *Advanced Materials*, vol. 16, no. 14, pp. 1151-1170, July 2004.

[5] U. Boudriot, R. Dersch, A. Greiner, J. H. Wendorff, "Tissue Engineering, Drug Delivery, Wound Healing via Polymer Nano Fibers and Nanotubes", *Artificial Organs*, vol. 30, pp. 785-792, Oct. 2006.

[6] D. Thassu, M. Deleers, Y. Pathak, "Particulate drug delivery systems", *Drug Development and Industrial Pharmacy*, vol. 34, no. 1, Jan. 2008.

[7] J. B. Melanko, M. E. Pearce, A. K. Salem, "Nanotubes, Nanorods, Nanofibers, and Fullerenes for Nanoscale Drug Delivery", *Nanotechnology in Drug Delivery*, vol. X, pp. 105-127, Oct. 2008.

[8] J. Zeng, X. Xu, X. Chen, Q. Liang, X. Bian, L. Yang, X. Jing, "Biodegradable electrospun fibers for drug delivery", *Journal of Controlled Release*, vol. 92, no. 3, pp. 227-231, Oct. 2003.

[9] E. Kenawy, F. I. Abdel-Hay, M. H. El-Newehy, G. E. Wnek, "Processing of polymer nanofibers through electrospinning as drug delivery systems", *Nanomaterials: Risks and Benefits*, pp. 247-263, Dec. 2008.

[10] G. Taylor, "Disintegration of water drops in an electric field," *Proceedings of the Royal Society of London, Series A, Mathematical and Physical Sciences*, vol. 280, no. 1382, pp. 383-397, Jul. 1964.

[11] S. L. Shenoy, W. D. Batesa, H. L. Frisch, and G. E. Wnek, "Role of chain entanglements on fiber formation during electrospinning of polymer solutions: good solvent, non-specific polymer–polymer interaction limit," *Polymer*, vol. 46, pp. 3372–3384, April 2005.

[12] S. Megelski, J. S. Stephens, D. B. Chase, J. F. Rabolt, "Micro- and nanostructured surface morphology on electrospun polymer fibers", *Macromolecules*, vol. 35, no. 22, pp. 8456-8466, Oct. 2002.

[13] H. Fong., I. Chun, D. H. Reneker, "Beaded nanofibers formed during electrospinning", *Polymer*, vol. 40, no. 16, pp. 4585-4592, July 1999.

[14] J. Kameoka, R. Orth, Y. Yang, D. Czaplewski, R. Mathers, G. Coates, H. G. Craighead, "A scanning tip electrospinning source for deposition of oriented nanofibers", *Nanotechnology*, vol. 14, no. 10, pp. 1124-1129, Oct. 2003.

[15] X. H. Zhong, K. S. Kim, D. F. Fang, S. F. Ran, B. S. Hsiao, B. Chu, "Structure and process relationship of electrospun bioabsorbable nanofiber membranes", *Polymer*, vol. 43, no. 16, pp. 4403-4412, July 2002.

[16] W. K. Son, J. H. Youk, T. S. Lee, W. H. Park, "Electrospinning of ultrafine cellulose acetate fibers: studies of a new solvent system and deacetylation of ultrafine cellulose acetate fibers", *J. Polymer Sci. B Polymer Phys.*, vol. 42, no. 1, pp. 5-11, Jan. 2004.
[17] J. S. Choi, S. W. Lee, L. Jeong, S. H. Bae, B. C. Min, J. H. Youk, W. H. Park, "Effect of organosoluble salts on the nanofibrous structure of electrospun poly (3-hydroxybutyrate-co-3-hydroxyvalerate)", *International Journal of Biological Macromolecules*, vol. 34, no. 4, pp. 249-256, Aug. 2004.
[18] W. K. Son, J. H. Youk, T. S. Lee, W. H. Park, "The effects of solution properties and polyelectrolyte on electospinning of ultrafine poly (ethylene oxide) fibers", *Polymer*, vol. 45, no. 9, pp. 2959-2966, April 2004.
[19] C. M. Hsu, S. Shivakumar, "N, N-dimethylformamide Additions to the Solution for the Electrospinning of Poly(e-caprolactone) Nanofivers", *Macromol. Mater. Eng.* vol. 289, pp. 334-340, April 2004.
[20] K. H. Lee, H. Y. Kim, H. J. Bang, Y. H. Jung and S. G. Lee, "The change of bead morphology formed on electrospun polystyrene fibers", Polymer, vol. 44, no. 14, pp. 4029-4034, June 2003.
[21] J. S. Lee, K. H. Choi, H. D. Ghim, S. S. Kim, D. H. Chun, H. Y. Kim, W. S. Lyoo, "Role of molecular weight of atactic poly(vinyl alcohol) (PVA) in the structure and properties of PVA nanofabric prepared by electrospinning", *J. Appl. Polym. Sci.*, vol. 93, no. 4, pp. 1638–1646, May 2004.
[22] C. J, Buchko, L. C. Chen, Y. Shen, D. C. Martin, "Processing and microstructural characterization of porous biocompatible protein polymer thin films", *Polymer*, vol. 40, no. 26, pp. 7397-7407, Dec. 1999.
[23] S. Zhao, X. Wu, L. Wang, Y. Huang, "Electrospinning of Ethyl-Cyanoethyl Cellulose/Tetrahydrofuran Solution", *Journal of Applied Polymer Science*, vol. 91, no. 1, pp. 242-246, Jan. 2004.
[24] J. M. Deitzel, J. Kleinmeyer, D. Harris, N. C. B. Tan, "The effect of processing variables on the morphology of electrospun nanofibers and textiles", *Polymer*, vol. 42, no.1, pp. 261-272, Jan. 2001.
[25] M. M. Demir, I. Yilgor, E. Yilgor, and B. Erman, "Electrospinning of polyurethane fibers," *Polymer*, vol. 43, no. 11, pp. 3303-3309, May 2002.
[26] T. Jarusuwannapoom, W. Hongrojjanawiwat, S. Jitjaicham, L. Wannatong, M. Nithitanakul, C. Pattamaprom, P. Koombhongse, R. Rangkupan, and P. Supaphol, "Effect of solvents on electro-spinnability of polystyrene solutions and morphological appearance of resulting electrospun polystyrene fibers", *European Polymer Journal*, vol. 41, no. 3, pp. 409–421, March 2005.
[27] G. C. Rutledge, Y. Li, S. Fridrikh, S. B. Warner, V. E. Kalayci, P. Patra, "Electrostatic spinning and properties of ultrafine fibers", *National Textile Cente*r, 2000 Annual Report, pp. 1-10, 2000.
[28] X. M. Mo, C. Y. Xu, M. Kataki, S. Ramakrishna, "Electrospun P(LLA-CL) nanofiber: a biomimetic extracellular matrix for smooth muscle cell and endothelial cell proliferation", *Biomaterials*, vol. 25, no. 10, pp. 1883-1890, May 2004.
[29] M. Bognitzki, W. Czado, T. Frese, A. Schaper, M. Hellwig, M. Steinhart, A. Greiner, J. H. Wendorff, "Nanostructured fibers via electrospinning", *Advanced Materials*, vol. 13, no. 1, pp. 70-72, Jan. 2001.

[30] Y. Lu, F. Zhou, W. Shui, L. Bian, Y. Guo, P. Yang, "Pulsed Electrospray for Mass Spectrometry", *Ana. Chem.*, vol. 73, no. 19, pp. 4748-4753, Oct. 2001.
[31] M. D. Paine, "Transient electrospray behaviour flowing high voltage switching", *Microfluidics and nanofluidics*, vol. 6, no. 6, pp. 775-783, June 2009.
[32] O. Yogi, T. Kawakami, M. Yamauchi, J. Y. Ye, M. Ishikawa, "Ondemand droplet spotter for preparing pico to femtoliter droplets on surfaces" *Ana. Chem*., vol. 73, no. 8, pp.1896–1902, April 2001.
[33] C. H. Chen, D. A. Saville, I. A. Aksay, "Scaling laws for pulsed electrohydrodynamic drop formation", *Appl. Phys. Lett.*, vol. 89, 124103, Sept. 2006.
[34] A. Jaworek, A. Krupa. M. Lackowski, A. Sobczyk, T. Czech, S Ramakrishna, S. Sundarrajan, D. Pliszka, "Nanocomposite fabric formation by electrospinning and electrospraying technologies", *Journal of Electrostatics*, vol. 67, no. 2-3, pp. 435-438, Feb. 2009.
[35] L. Heinemann, K. Porle, P. Ranstad, "Design of a high power pulse voltage generator for electrostaticprecipitators using magnetic switching technique", *APEC '97 Conf.*, vol. 2, pp. 948-952, Feb. 1997.
[36] N. A. Yvorovsky, S. S. Peltsman, J. I. Komev, Yu. V. Volkov, "Technology of water treatment using pulsed electric discharges", *Science and Technology Korus 2000*, vol. 3, pp. 422-427, June-July 2000.
[37] D. Campbell, J. Harper, V. Natham, F. Xiao, R. Sundararajan, "A Compact High Voltage Nanosecond Pulse Generator", *Proc. ESA Annual Meeting on Electrostatics 2008*, Paper H3, June 2008.
[38] L. P´ecastaing, J. Paillol, T. Reess, A. Gibert, P. Domens, "Design and performance of high voltage pulse generators for ultra-wideband applications", *Meas. Sci., Technol.*, vol. 12, no. 10, pp. 1718–1725, Oct. 2001.
[39] J. H. Kim, B. D. Min, S. V. Shenderey, G.H. Rim, "High Voltage Pulsed Power Supply Using IGBT Stacks", *IEEE Trans. Dielectrics and Electrical Insulation*, vol. 14, no. 4, pp. 921-926, Aug., 2007.
[40] J. R. Grenier, "Design of a Mosfer-based Pulsed Power Supply for Electroporation", M. ASc. Thesis, University of Waterloo, Waterloo, ON, Canada, 2006.
[41] N. Mohan, T. Undeland, W. Robbins, *Power Electronics: Converter, Application and Design*, 3rd Edition, John Wiley & Sons. inc., 2003.
[42] S. Castagno, R. D. Curry, "Analysis and Comparison of a Fast Turn-On Series IGBT Stack and High-Voltage-Rated Commercial IGBTs", *IEEE Trans. Plasma Science*, vol. 34, no. 5, pp. 1692-1696, Oct. 2006.
[43] Powerex, Inc.,▪2009 [Online]. Available: http://www.pwrx.com/Home.aspx [Accessed: 2009]
[44] IXYS Corporation,▪2009 [Online]. Available: http://www.ixys.com/index.asp [Accessed: 2009]
[45] M. H. Rashid, *Power Electronics: Circuits Devices, and Application*, 3rd Edition, Prentice Hall, 2004.
[46] LM555 timer▪National Semiconductor [Online]. Available: www.national.com/ds/LM/LM555.pdf [Accessed: 2009]
[47] J. Segura, C. F. Hawkins, *MOS Electronics: How It Works, How It Fails*, Wiley-IEEE Press, 2004.

[48] Z. M. Huang, Y. Z. Zhang and M. Kotaki, “A review on polymer nanofibers by electrospinning and their applications in nanocomposites”, *Compos Sci Technol*, vol.63, no. 15, pp.2223-2253, Nov. 2003.
[49] R. J. Spontak, T. K. Ghosh, H. Boerner, X. Sun, R. Shankar, “Single-step protein surface-attachment to electrospun fibers”, *National Textile Center Annual Report*, Nov., 2004.
[50] A. Atala, R. P. Lanza, “Methods of tissue engineering”, *Academic Press USA*, 2002.
[51] R. Glicklis, L. Shapiro, R. Agbaria, J. C. Merchuk, S. Cohen, “Hepatocyte behavior within three-dimensional porous alginate scaffolds”, *Biotechnol Bioeng*, vol.67, no. 3, pp.344-353, Feb. 2000.
[52] T. W. Chung, J. Yang, T. Akaike, K. Y. Cho, J. W. Nah, S. I. Kim, C. S. Cho, “Preparation of alginate/galactosylated chitosan scaffold for hepatocyte attachment” *Biomaterials*, vol.23, no. 14, pp.2827-2834, July 2002.
[53] J. A. Rowley, D. J. Mooney, “Alginate type and RGD density control myoblast phenotype”, *J Biomed Mater Res*, vol.60, no. 2, pp.217-223, May 2002.
[54] J. W. Lua, Y. L. Zhua, Z. X. Guoa, P. Hua, J. Yu, “Electrospinning of sodium alginate with poly(ethylene oxide)”, *Polymer*, vol.47, no. 23, pp.8026-8031, Oct. 2006.
[55] D.A. Grant, J. Gowar, *Power MOSFETs Theory and Applications*, John Wiley&Sons, 1989.
[56] Y. Kooa, J. Kima, W. Choa, and H. Chung, “Investigation of resistance change characteristics with applied electric field on Ag/chalcogenide As2S3 and As40Ge10Se15S35 thin film structure”, *32nd International Conf. on Micro- and Nano-Eng.*, vol.84, no. 5-8, pp. 1652-1655, May-August 2007.
[57] W. Zuo, M. Zhu , W. Yang, H. Yu, Y. Chen, Y. Zhang, “Experimental study on relationship between jet instability and formation of beaded fibers during electrospinning”, *Polymer Engineering and Science*, vol. 45, no. 5, pp. 704-709, March 2005.
[58] C. Zhanga, X. Yuana, L. Wua, Y. Hana, J. Shenga, “Study on morphology of electrospun poly(vinyl alcohol) mats”, *European Polymer Journal*, vol. 41, no. 3, pp. 423-432, March 2005.
[59] Y. M. Shin, M.M. Hohman, M.P. Brenner, G.C. Rutledge, “Electrospinning: A Whipping Fluid Jet Generates Submicron Polymer Fibers” *Appl. Phys. Lett.*, vol. 78, no. 8, pp.1149-1150, 2001.
[60] D.A. Saville, “Stability of electrically charged viscous cylinders”, *Phys. Fluids*, vol. 14, pp. 1095-1099, June 1971.
[61] G. I. Taylor, “Disintegration of water drops in an electric field”, *Proc. R. Soc. London Ser.*, A 280, pp. 383–397, 1964.
[62] T. Uyara, F. Besenbacher, “Electrospinning of cyclodextrin functionalized polyethylene oxide (PEO) nanofibers”, *European Polymer Journal*, vol. 45, no. 4, pp. 1032-1037, April 2009.
[63] L. Lia, Y. L. Hsieh, “Chitosan bicomponent nanofibers and nanoporous fibers”, *Carbohydrate Research*, vol. 341, issue 3, pp. 374-381, Feb. 2006.
[64] R. Mincheva, N. Manolova, D. Paneva, I. Rashkov, “Preparation of polyelectrolyte-containing nanofibers by electrospinning in the presence of a non-ionogenic water-soluble polymer”, *J Bioact Compat Polym*, vol. 20, no. 5, pp. 419–435, 2005.
[65] C. Angammana, “Investigation of the optimum electric field and working range for stable electrospinning”, *Cage club*, Aug. 2009.